Efficient and selective removal of Se^{VI} and As^{V} mixed contaminants from aqueous media by montmorillonite-nanoscale zero valent iron nanocomposite

Jonathan Suazo-Hernández[a,b], Karen Manquián-Cerda[c], María de la Luz Mora[b,d], Mauricio Molina-Roco[e], María Angélica Rubio[c,f], Binoy Sarkar[g*], Nanthi Bolan[h], Nicolás Arancibia-Miranda[c,f*]

[a] Programa de Doctorado en Ciencias de Recursos Naturales, Universidad de La Frontera, Av. Francisco Salazar 01145, P.O. Box 54-D, Temuco, Chile

[b] Center of Plant, Soil Interaction and Natural Resources Biotechnology, Universidad de La Frontera. UFRO. Temuco, 4780000, Chile

[c] Facultad de Química y Biología, Universidad de Santiago de Chile, Av. B. O'Higgins, 3363, Santiago, Chile

[d] Departamento de Ciencias Químicas y Recursos Naturales, Universidad de La Frontera, Av. Francisco Salazar 01145, P.O. Box 54-D, Temuco, Chile

[e] Escuela de Agronomía, Universidad Mayor, Camino La Pirámide #5750, Huechuraba, Santiago 8580745, Chile

[f] Center for the Development of Nanoscience and Nanotechnology, CEDENNA, 9170124, Santiago, Chile

[g] Lancaster Environment Centre, Lancaster University, Lancaster, LA1 4YQ, UK

[h] Global Centre for Environmental Remediation, University of Newcastle, Callaghan, NSW 2308, Australia

* Corresponding author: Dr Binoy Sarkar; Lancaster University; e-mail: b.sarkar@lancaster.ac.uk

Co-corresponding author: Dr Nicolás Arancibia-Miranda; Universidad de Santiago de Chile; e-mail: nicolas.arancibia@usach.cl

ABSTRACT

Nanoscale zero-valent iron (NZVI) and NZVI supported onto montmorillonite (NZVI-Mt) were synthetized and used in this study to remove Se^{VI} and As^{V} from water in mono- and binary-adsorbate systems. The adsorption kinetics and isotherm data for Se^{VI} and As^{V} were adequately described by the pseudo-second-order (PSO) (r^2>0.94) and Freundlich (r^2>0.93) equations. Results from scanning electron microscopy showed that the dimension of the NZVI immobilized on the Mt was smaller than pure NZVI. Using 0.05 g of adsorbent and an initial 200 $mg \cdot L^{-1}$ As^{V} and Se^{VI} concentration, the maximum adsorption capacity (q_{max}) and partition coefficient (PC) for As^{V} on NZVI-Mt in monocomponent system were 54.75 $mg \cdot g^{-1}$ and 0.065 $mg \cdot g^{-1} \cdot \mu M^{-1}$, which dropped respectively to 49.91 $mg \cdot g^{-1}$ and 0.055 $mg \cdot g^{-1} \cdot \mu M^{-1}$ under competitive system. For Se^{VI} adsorption on NZVI-Mt in monocomponent system, q_{max} and PC were 28.63 $mg \cdot g^{-1}$ and 0.024 $mg \cdot g^{-1} \cdot \mu M^{-1}$, respectively. Values of q_{max} and PC were higher for NZVI-Mt than NZVI and montmorillonite, indicating that the nanocomposite contained greater adsorption sites for removing both oxyanions, but with a marked preference for As^{V}. Future research should evaluate the effect of different operational variables on the removal efficiency of both oxyanions by NZVI-Mt.

Keywords: NZVI; Water treatment; Arsenic and selenium removal; Competitive adsorption; Partition coefficient

1. Introduction

In recent years, the presence of trace elements (TEs) in aquatic environments has been a major concern due to their adverse effects on aquatic life, animals, plants, and humans (Tofighy and Mohammadi, 2011). In this context, arsenic (As) and selenium (Se) are present in water systems and soils in trace concentrations but can be extremely hazardous when encountered in high concentrations (Jackson and Miller, 2000; Wilkin et al., 2018). The main sources of Se are carbon shales, phosphatic rocks, coals and minerals like Se-bearing chalcopyrites ($CuFe(Se,S)_2$), pyrites ($Fe(Se,S)_2$), klockmannite (CuSe), krutaite ($CuSe_2$) and mandarinoite ($Fe_2(SeO_3)_3{\cdot}6H_2O$) (Bajaj et al., 2011; Zhu et al., 2012). Similarly, As is found in minerals such as tennantite, $(Cu,Fe)_{12}As_4S_{13}$, enargite (Cu_3AsS_4), arsenopyrite (FeAsS), among others (Nazari et al., 2017). In recent years, incorporation of both the elements in their inorganic forms to aqueous matrices has been favored by anthropogenic activities such as agriculture, mining, thermoelectric, oil refineries, etc., causing an increase of their concentrations in surface and groundwater, giving rise to pollution scenarios in countries such as Chile, Argentina, New Zealand, Bangladesh, India, , the United States and Japan (Huq et al., 2006; Barati et al., 2010; Neupane et al., 2014; He et al., 2018). This environmental problem has increased the incidence of diseases in the population, where it has been reported that the ingestion of Se >1 $mg{\cdot}kg^{-1}$ in the human body through food can cause numbing of fingers and toes, damage to kidney and liver tissues, loss of hair and nails, as well as carcinogenesis (Rovira et al., 2008; Santos et al., 2015; Xie et al., 2015). Similarly, long-term exposition to As elevates the risk of cancer of the kidney and

bladder, in addition to producing skin pigmentation, diabetes, and lung ailments (Impellitteri, 2004; Luther et al., 2012). For this reason, the World Health Organization (WHO) suggested that concentrations in drinking water should not exceed 40 ppb for Se (Santos et al., 2015), and 10 ppb for As (Wang et al., 2014).

Various studies have focused on the development and application of nanoparticles that allow mitigating environmental problems, specially remediating aquatic contaminants (Kanel et al., 2005; Martinson and Reddy, 2009; Sun et al., 2014; Jain et al., 2015). An example of such materials is nanoscale zero-valent iron (NZVI) (Otyepka, 2014; Peng et al., 2017), which in addition to having low production cost has high effectiveness in the elimination/removal of organic and inorganic contaminants from aquatic systems. The NZVI has been shown to successfully remove contaminants such as Orange II (Luo et al., 2013), 1,1,1-trichloro-2,2-bis(p-chlorophenyl) ethane (El-Temsah et al., 2013), Cd^{2+} (Zhang et al., 2014), Pb^{2+} (Arancibia-miranda et al., 2014), As^{III} and As^{V} (Kanel et al., 2005; Sun et al., 2011; Suazo-Hernández et al., 2019), and Se^{IV} and Se^{VI} (Ling et al., 2015; Xie et al., 2017). The NZVI can form a core/shell structure whose shell is constituted of iron oxides and/or (oxy)hydroxides, such as magnetite, maghemite, goethite, which in turn together with the metallic iron core are responsible for diverse mechanisms for pollutant elimination by NZVI nanoparticles. The mechanisms include precipitation, co-precipitation, redox and adsorption processes (Yan et al., 2012; Ling et al., 2015), which contribute to the high contaminant removal capacities by this nanomaterial.

Recently, the support/immobilization of NZVI on substrates like zeolite, biochar, kaolinite, montmorillonite and palygorskite has arisen as an economic alternative for improving the performance of NZVI via preventing the aggregation of nanoparticles while increasing the BET-specific surface area (Zhang et al., 2011; Kim et al., 2013; Xi et al., 2014; Arancibia-Miranda et

al., 2016; Lin et al., 2017; Fan et al., 2019; Suazo-Hernández et al., 2019). This has expanded NZVI's applications in extreme environmental conditions like acidic pH, high ionic strength, and under the presence of coexisting ions. Among the support materials for the nanoparticles, montmorillonite (Mt) stands out as it is an expandable clay mineral (2:1) having excellent ability to attract cations due to its permanent negative charge (Zhu et al., 2015). Arancibia-Miranda et al. (2016) reported that immobilizing NZVI on Mt (NZVI-Mt) enabled a 2.3 times increase of Pb^{2+} removal compared to pristine NZVI, while Pang et al. (2014) showed that the NZVI-Mt composite had twice the surface area of NZVI, increasing the degradation of decabromodiphenyl ether. However, the adsorption efficiency of the NZVI-Mt composite is dependent on the chemical environment of the medium as well as on the adsorbing surface, media pH, and particularly the presence of anions and cations in the aqueous system (Dąbrowski et al., 2005; Hiemstra et al., 2010), which may give rise to a competitive effect, decreasing and even preventing the pollutant of interest from being removed by the adsorbent. Based on these phenomena, recently Li et al. (2017) observed that the zeolite-NZVI composite (Z-NZVI) decreased its Cd^{2+} removing capacity from 62.0 to 32.9, and 5.9 $mg \cdot g^{-1}$ in the presence of As^{III} and Pb^{2+}, respectively.

There have been studies about the preparation, characterization and elimination of contaminants by clay-NZVI nanocomposites. However, the removal of contaminants in a competitive chemical environment, especially in the presence of other similar or heterogeneous compounds or ions, is a least reported area. The effects of the presence of two oxyanions such as selenate (Se^{VI}) and arsenate (As^{V}) in mono-component and competitive systems on the removal of these contaminants by clay-NZVI have not been realized yet. Thus, our goal was to support nZVI on montmorillonite clay mineral (Mt) (NZVI-Mt), characterize and evaluate its Se^{VI} and As^{V}

removal capacities and partition coefficients, and comparing the values to that of NZVI and Mt (pristine material). Finally, through the characterization of the adsorbents conducted pre- and post-adsorption experiments, a plausible mechanism for the removal process of As^{V} in the absence and presence of Se^{VI} was proposed.

2. Experimental

2.1. Chemicals

The reagents used were $FeCl_3 \cdot 6H_2O$, NaCl, $NaBH_4$, NaOH, and HCl, all of analytical grades (Merck). Montmorillonite (Mt) clay mineral was acquired from Sigma-Aldrich. As_2O_5 (1000 $mg \cdot L^{-1}$) standard reference solution (Tritrisol, Merck, Germany) and Na_2SeO_4 analytical grade (Sigma-Aldrich) were used to validate the measurements.

2.2. Synthesis of nanoadsorbents

The NZVI nanoparticles were synthesized using $NaBH_4$ as the reducing agent. $NaBH_4$ (1.6 M) was added dropwise to a 1.0 M $FeCl_3 \cdot 6H_2O$ solution at 25 ± 2 ^{o}C, in a N_2 atmosphere with mechanical stirring. The reduction reaction is represented by the following Eq. 1 (Kanel et al., 2005).

$$4Fe^{3+} + 3BH_4^- + 9H_2O \rightarrow 4Fe^0 + 3H_2BO_3^- + 6H_2 \uparrow + 12H^+ \qquad \text{(Eq. 1)}$$

The NZVI-Mt nanocomposite had a theoretical 1:2 ratio of NZVI:Mt (% w/w), and it was prepared following the methodology described by Wang and Zhang (1997) with some modifications. The Mt (100 g) was first homoionized by treating the clay mineral with 200 mL of $NaNO_3$ (0.5 M) for seven days, separated the solid phase, and freeze-dried for further use. For the immobilization of nanoparticles, 1.0 g of $FeCl_3 \cdot 6H_2O$ was dissolved in 250 mL of Milli Q

water, and homoionized Mt was suspended in the same solution. The mixture (Mt-Fe^{3+}) was ultrasonicated for half an hour, and stirred for 180 min at 25 ± 2 ºC. For a complete reduction of Fe^{3+}, 25 mL of $NaBH_4$ solution (1.6 M) was added gradually over five min. Later, an ultracentrifuge was used to separate the NZVI-Mt from the suspension at 9000 rpm for 10 min, and washed three times with a water-ethanol (1:1) mixture. This was done to remove the residual salts, and to avoid NZVI oxidation. Finally, the nanocomposite was freeze-dried, and stored at -4ºC in a freezer until further use.

2.3. Characterization of adsorbents

The adsorbent materials were characterized before and after the adsorption reaction. The x-ray diffraction (XRD) measurement was conducted using a powder diffractometer (Shimadzu XRD-6000) at 1.5418 Å with CuKα radiation in the 2θ region of 5-80º. Scanning electron microscopy (SEM) was carried out with a FEI Nova Nano SEM 200 equipment, and particle sizes were analyzed using the commercial software ImageJ. The BET-specific surface area (SSA) of adsorbents was obtained using the BET method (Brunauer–Emmett–Teller) with a Quantachrome 1200 Nova Station equipment. The zeta potential (ZP) was measured in the presence of 200 mL NaCl (0.01 M) using Zeta Meter ZM4 apparatus, and the isoelectric point (IEP) was obtained from graphs of ZP versus pH.

2.4. Batch adsorption studies

The influence of initial pH values on the removal capacity of Se^{VI}, As^{V} or Se^{VI} - As^{V} on Mt, NZVI and NZVI-Mt in the mono-component and the competitive system was determined with 20 mL of analyte solutions (200 mg·L^{-1}) mixed with 50 mg of material in 50 mL polypropylene

tubes at a pH range of 3 to 10, and in 0.01 M NaCl solution as a background electrolyte. The tubes were stirred for 1,440 min in an orbital shaker at 180 rpm and 25 ± 2 ºC. Later, to determine the variation of post-experimental pH, values were measured in the filtered solution using a pH meter after the adsorption experiment.

The adsorption kinetics of Se^{VI} and As^{V} in the mono-component and competitive system was studied with 20 mL of each oxyanion (200 mg·L^{-1}) using 50 mg of adsorbents in 50 mL polypropylene tubes at pH = 7.0 ± 0.2, and in 0.01 M NaCl solution as a background electrolyte. A set of suspensions were stirred at different time intervals (5 - 180 min) in an orbital shaker at 180 rpm and 25 ± 2 ºC.

The experimental adsorption isotherms of oxyanions in the mono-component and competitive system were conducted with 50 mg of material in 50 mL polypropylene tubes with 20 mL at different initial concentrations of Se^{VI} and As^{V} (0.5, 1, 5, 10, 30, 60, 100, 150 and 200 mg·L^{-1}) in 0.01 M NaCl solution as the background electrolyte, and at pH = 7.0 ± 0.2. The suspensions were stirred for 360 min in an orbital shaker at 180 rpm and 25 ± 2 ºC.

All the samples were centrifuged on a Sorvall Model RC-5B Plus centrifuge for 10 min at 8000 rpm. The supernatants were filtered using syringe filters (0.22 µm), and after filtration, the quantification of total selenium (Se_{total}) and arsenic (As_{total}) was made using a Thermo SOLAAR-M6 atomic absorption spectrometer. The specific amounts of Se^{VI} and As^{V} (q_e, mg·g^{-1}) adsorbed were determined using Eq. 2

$$q_e = \frac{(C_0 - C_t)V}{w} \qquad \text{(Eq. 2)}$$

where, C_o is the initial concentration of Se^{VI} or As^{V}, C_t is the concentration of Se^{VI} or As^{V} at time t or the equilibrium concentration (mg·L^{-1}), w is the weight (g) of the adsorbent, and V is the volume (L). Adsorption experiments were checked by carrying out triplicate analyses.

2.5 Data analysis

The mathematical kinetic and isotherm equations used in this study are presented in Supplementary Information (SI; Table S1 and S2). The fitness of kinetic and isotherm equations was evaluated by considering standard deviation and the statistical parameters such as linear coefficient of determination (r^2) and chi-squared value (χ^2) (Boparai et al., 2011; Arancibia-Miranda et al., 2016) (SI).

3. Results and discussion

3.1. Characterization of nanoadsorbents

The XRD diffractograms of NZVI and NZVI-Mt pre- and post-adsorption are shown in Fig. 1. For NZVI (Fig. 1a), two characteristic reflections of αFe at 2θ = 44.7º and 65.0º were seen (Kanel et al., 2005; Suazo-Hernández et al., 2019). For the Mt (Fig. S1a) and NZVI-Mt (Fig. 1b), the reflections at 12.63 Å (002), 4.44 Å (101) and 2.56 Å (107) represented the pattern of Na-exchanged montmorillonite ($Na_{0.3}(Al,Mg)_2Si_4O_{10}$ $8H_2O$) (Yuan et al., 2009; Arancibia-Miranda et al., 2016). Additionally, the reflection at 3.34 Å (005) indicated the presence of illite ($KAl_4(Si,Al)_8O_{10}(OH)_4)_4H_2O$) in the clay mineral sample (Arancibia-Miranda et al., 2016). A slight change of the main diffraction peak of the NZVI was seen in the nanocomposite, where the αFe^0 diffraction angle (2θ) was shifted from 44.7º to 45.5º, in agreement with previous reports (Pang et al., 2014), suggesting that this shift corresponded to a decrease of the crystallite size of NZVI (Yucelen et al., 2012; Arancibia-Miranda et al., 2017).

During the reaction with Se^{VI}, As^{V}, and Se^{VI} - As^{V}, the NZVI showed new diffraction peaks characteristic of iron oxides. For instance, with Se^{VI} (Fig. 1c), magnetite (Fe_3O_4) and/or maghemite(γ-Fe_2O_3) peak was seen at 2θ = 35.8º, and lepidocrocite (γ-FeOOH) at 2θ = 27.1º, in

addition to decrease of the αFe^0 signal associated with loss of the crystalline structure (Suazo-Hernández et al., 2019). For NZVI-Mt treated with Se^{VI} and As^V, the αFe^0 signal practically disappeared, and no new signal was observed. During the treatment of Se^{VI} - As^V, only NZVI showed a different behavior; the presence of both oxyanions decreased the degree of oxidation of the outer shell, showing only magnetite-maghemite precipitated (Fig. 1g). Therefore, the XRD results suggested that the support of NZVI on Mt changed the crystallinity of these nanoparticles because an amorphous oxide layer was formed on their surfaces after anion adsorption.

To understand the dimensions and morphologies of the nanomaterials, pre- and post-adsorption samples were investigated by SEM. Fig. 2a and 2b show that the pristine NZVI particles were larger in size than those immobilized on Mt (SEM images of pristine Mt are shown in Fig. S2a), likely due to the three-dimensional growth limitation of these nanoparticles when interacting with the clay mineral (Jia et al., 2018; Suazo-Hernández et al., 2019). The particle sizes found for NZVI and NZVI-Mt were between 50-190 nm and 30-170 nm, respectively (Fig. S3). The nanoparticles had a clear collar type shape, associated with each other via magnetic forces and van der Waals and electrostatic interactions that occurred due to the surface oxidation process (Sun et al., 2011; Arancibia-Miranda et al., 2016), as also indicated by the XRD results. The SSA of NZVI-Mt increased 7.9 and 25.5 times compared to that of NZVI and Mt, respectively, due to the accumulation of nanoparticles on the clay mineral (Table S3). After the oxyanion adsorption reactions, the size of iron nanoparticles was increased in NZVI and NZVI-Mt (Fig. 2c-h), likely due to the formation of different iron oxide coatings (Bhowmick et al., 2014; Trujillo-Reyes et al., 2014; Li et al., 2015).

3.2. Adsorption experiments

3.2.1. pH dependence

Solution pH is important on the adsorption process because the variation of pH influences the speciation of Se^{VI} and As^{V} in the solution as well as the ionization of the surface groups of the adsorbent materials. Fig. 3a shows that pH did not affect Se^{VI} removal by NZVI, with a maximum amount removed close to 57.0 $mg \cdot g^{-1}$ (70.0 %) at pH = 3. On the other hand, NZVI-Mt removed an amount of Se^{VI} close to 20.0 $mg \cdot g^{-1}$ (24.8 %) at pH = 3. The negligible effect of pH change on Se^{VI} removal using both the adsorbents might be related to the fact that under our experimental conditions there were no changes in oxidation states of the Se^{VI} species (Fig. S4a). The predominant interaction during the adsorption of Se^{VI} would have been a chemical mechanism (ligand exchange) because the adsorption was independent of the solution's pH (Xia et al., 2017a). The Mt reached a removal capacity of only 4.5 $mg \cdot g^{-1}$ of Se^{VI}, quite lower than NZVI and NZVI-Mt (Fig. 3a). The low adsorption of Se^{VI} by the pristine clay mineral was associated to the electrostatic repulsion generated between the permanent negative charges on Mt and Se^{VI} oxyanion (Charlet et al., 2007). Furthermore, this study showed that the coexistence of As^{V} affected the removal capacity of Se^{VI}. At pH = 3, the Se^{VI} adsorption capacity decreased from 55.46 to 43.89 $mg \cdot g^{-1}$ for NZVI, and from 19.79 to 4.59 $mg \cdot g^{-1}$ for NZVI-Mt (Fig. 3c), corresponding to a decrease of 14% and 19%, respectively, in the presence of As^{V}.

The changes in the removal of As^{V} as a function of pH was greater by NZVI than by the NZVI-Mt composite (Fig. 3b), where an increasing pH to values greater than the IEP (Fig. S5) decreased the adsorption capacity of the adsorbents. The pH response of NZVI-Mt would be related to the increase of the amount of surface negative charges with increasing pH, causing an increase in the electrostatic repulsion between the adsorbent and adsorbate (Suazo-Hernández et al., 2019). Due to pKa_2 for H_3AsO_4 is 6.7, at higher pH, the $HAsO_4^{2-}$ species start becoming

predominant in the solution (Fig. S4b) and electrostatic interaction between the adsorbent and As^V became less favored (Wang et al., 2014).

The data obtained for the As^V elimination with NZVI and NZVI-Mt in a competitive system were similar to those obtained for the mono-component system (Fig. 3d), which could be attributed to two factors. Firstly, the competing species Se^{VI} did not have a great affinity for the surface groups of the NZVI and NZVI-Mt (≡SiOH, ≡AlOH, $\equiv FeOH_2^+$, ≡FeOH, and $\equiv FeO^-$). This explanation was corroborated by the values of specific rate (k) and affinity (n) constants obtained in the kinetic and isotherm investigations, respectively, and also by the values of partition coefficients (PC), which are described in later sections. Secondly, the As^V species ($H_2AsO_4^-$, $HAsO_4^{2-}$ and AsO_4^{3-}) when forming chemical interactions (of greater affinity) with the surface groups could displace the previously adsorbed Se^{VI} species (Bhowmick et al., 2014). This is in agreement that the As^V species have the ability to form inner spheres complexes with the surface groups of NZVI in the presence of other anionic species such as NO_3^-, SO_4^{2-}, PO_4^{3-}, and HCO^- (Kanel et al., 2005; Tanboonchuy et al., 2012; Bhowmick et al., 2014).

To understand the adsorption mechanisms of both the oxyanions on the adsorbent surfaces, the pH variation ($\Delta pH = pH_{final}-pH_{initial}$) was plotted against the initial pH values (Fig. 4a-c). The results indicated that at $\Delta pH > 0$, there was a release of OH^-, giving an increase in the solution's pH_{final}. The opposite phenomenon was seen when $\Delta pH < 0$, implying a greater release of H^+ from the surface of the adsorbents, decreasing the pH_{final}.

Fig. 4a shows that at $pH_{initial} \geq 4.0$, the pH_{final} of the post-adsorption Se^{VI} solution on NZVI-Mt and NZVI tended to remain at pH 4.0, in contrast with the slightly higher pH_{final} (pH = 5) registered for the adsorption on Mt. This pH variation might be attributed to the *in situ* oxidation process undergone by Fe^0 (in NZVI and NZVI-Mt), which would have caused the release of H^+

into the bulk of the solution, and the formation of different surface Fe oxides on which Se^{VI} could be adsorbed (Fig. 2c and 2d). This process was independent of the solution's $pH_{initial}$, as confirmed by the effect of pH results (Fig. 3a). In relation to this process, Xia et al. (2017b) indicated that at pH < 7, the NZVI after being in contact with Se^{VI} released H^+ into the solution according to Eq. 2, 3, and 4:

$$Fe^0 + 2H^+ \rightarrow Fe^{2+} + H_2^{\uparrow} \quad \text{(Eq. 2)}$$

$$2H_2 + SeO_4^{2-} + 4H^+ \rightarrow Se_{\downarrow}^0 + 4H_2O \quad \text{(Eq. 3)}$$

$$3Fe^0 + 4Fe^{2+} + 4Se^0 + 4H_20 \rightarrow Fe_3O_4 + 4FeSe + 8H^+ \quad \text{(Eq. 4)}$$

Considering Eq. 3, it was probable that Se^{VI} displaced the equilibrium toward the formation of products in Eq. 4, in contrast with the effect produced after the adsorption of As^V on NZVI and NZVI-Mt (Bhowmick et al., 2014). It was because when adsorption of As^V on NZVI-Mt at $pH_{initial} < 9$ occurred, the pH_{final} remained close to 8 (Fig. 4b). This phenomenon might be associated with the fact that As^V anions were coordinated through ligand exchange with the surface ≡FeOH groups present in NZVI-Mt, releasing OH^-groups. An opposite behavior was seen when As^V adsorption by NZVI took place. In this case, at $pH_{initial} \geq 5.0$, ΔpH was -2, pointing to a greater generation of H^+ in the medium, and this might be related to the deprotonation of the predominant H_3AsO_4 species at that pH ($H_2AsO_4^- \leftrightarrow H^+ + HAsO_4^{2-}$). The ΔpH values for the competing system (Fig. 4c) showed a trend similar to that of the As^V adsorption system, suggesting that the reactions taking place in the solid-solution interface were dependent only on the presence of As^V.

3.2.2. Kinetics of adsorption

The experimental kinetic adsorption data of both oxyanions in mono-component and competition systems are presented in Table S4, and their trend is shown in Fig. 5. The equilibrium time for Se^{VI} adsorption on NZVI and NZVI-Mt reached during the first 5 and 20 min, respectively, with the removed amount almost three times greater for NZVI-Mt than the pristine NZVI (Fig. 5a). The equilibrium contact time for the adsorption of As^{V} on NZVI in both systems occurred within 40 min of contact, while for the NZVI-Mt composite it occurred at 90 min (Fig. 5b and 5d), with the removed amount 2.5 times greater for the nanocomposite compared to NZVI in a mono-component system, and 2.0 times greater in the competition system (Table 1).

These results show that the support of NZVI on Mt, besides increasing the SSA (Table S3), favored the removal of Se^{VI} in a mono-component system, and of As^{V} in both mono- and competitive systems (Fig. 5a-d). This explanation could be associated to the higher amount of surface functional groups (≡Fe-OH and ≡Fe-O-OH) which were generated by the functionalization of the clay mineral with NZVI (Suazo-Hernández et al., 2019). Additionally, the times taken for the saturation of the surface functional groups in NZVI-Mt with As^{V} were the same in both the mono-solute and competitive systems, and consequently the coexistence of Se^{VI} did not interfere with As^{V} adsorption by this adsorbent.

PC in a solid/liquid adsorption system correspond to the ratio of adsorbate concentration in and on the solid adsorbent phase to its concentration in the liquid phase at equilibrium (Hu et al., 2014; O'Connor and Connolly, 1980). PC was used to characterize the adsorption affinity of adsorbents (Ahmed et al., 2016; Na et al., 2019), and could help to corroborate and understand the effect of competing species on oxyanion adsorption, which is conventionally evaluated by model fitting. The PC values obtained at different reaction times (5 - 180 min) for the adsorption of As^{V} on Mt and NZVI in competing system fluctuated between 0.0024 - 0.0030 $mg \cdot g^{-1} \cdot \mu M^{-1}$,

and 0.007 - 0.016 $mg \cdot g^{-1} \cdot \mu M^{-1}$, respectively. These values were similar to those determined in single-component system, indicating that Se^{VI} did not notably alter the adsorption of As^{V} on Mt and NZVI (Table S5). Meanwhile, the decrease of PC values for As^{V} adsorption on NZVI-Mt in the competing system (PC = 0.019 - 0.060 $mg \cdot g^{-1} \cdot \mu M^{-1}$) compared to single-component system (PC = 0.020 - 0.097 $mg \cdot g^{-1} \cdot \mu M^{-1}$) suggested that As^{V} adsorption was hampered on NZVI-Mt by the presence of Se^{VI} (Table S5). It was not possible to report the PC for Se^{VI} in a competing system because the adsorbents showed negligible adsorption, suggesting that As^{V} was an interferer during the overall kinetic process.

Higher PC values were obtained for Se^{VI} adsorption on Mt-NZVI than NZVI and Mt at different reaction times in single-component system. PC values were greater for As^{V} adsorption on Mt-NZVI in both single and competing systems. These results could be attributed to a synergistic effect where a uniform dispersion of NZVI particles were obtained on Mt during the immobilization of nanoparticles on the clay mineral (Kim et al., 2019). In other words, there was an increase in the number of adsorption sites after immobilization of NZVI on Mt. A decrease in PC value was expected in the competing As^{V} - Se^{VI} / NZVI-Mt system with respect to single-component system (because Se^{VI} would be occupying the adsorption sites), which did not occur. This inconsistency would be a consequence of Mt exfoliation likely to occur during the NZVI immobilization process using harsh chemicals (Lee and Ko, 2014; Prasanth et al., 2013), which might favor NZVI passivation and alter the adsorption sites.

Pseudo-second-order (PSO) and pseudo-first-order (PFO) equations (Table 1) were used to describe the kinetic experimental results. According to these equations, we obtained adsorption capacity parameters and rate constants for Se^{VI} and As^{V} for the different adsorbents and systems. The obtained kinetic parameters suggested that both the equations were capable of describing the

experimental data of Se^{VI} removal onto NZVI and NZVI-Mt in the mono-component system with high r^2 values and low χ^2 differences (Table 1). The PSO model gave a greater closeness between experimental (q_e,exp) and theoretical (q_e,cal) adsorption capacity values than PFO model, indicating a chemisorption process (Barkat et al., 2009). Since Se^{VI} (SeO_4^{2-}) anion has a tetrahedral structure whose O-Se bond distance is 1.61-1.65 Å (Fernández-Martínez and Charlet, 2009), so it was probable that the adsorption predominantly occurred through the formation of bidentate complexes (Peak, 2006; Chan et al., 2009). However, a few studies indicated that the species with tetrahedral structure could also coordinate with the surface groups of an adsorbent through the formation of monodentate complexes (Ling et al., 2015; Arancibia-Miranda et al., 2016; Xia et al., 2017a; Xie et al., 2017).

The adsorption kinetics of As^V onto NZVI and NZVI-Mt in the mono-component system (r^2 = 0.988 and 0.996, respectively) as well as under Se^{VI} competition (r^2 = 0.981 and 0.996, respectively) best fitted to the PSO equation (Table 1), indicating that the adsorption of As^V took place mainly through formation of bidentate inner-sphere complexes (Zhang et al., 2005; Limousin et al., 2007; Sun et al., 2011). The kinetics of As^V adsorption onto NZVI might be explained considering that initially it was adsorbed on the NZVI surface. After the outer surface of NZVI became saturated with As^V, it would pass through the iron oxide layers, and would be retained in the inner surface of the nZVI. This phenomenon might also be favored in NZVI-Mt by the presence of Mt because of the laminar structure of the clay mineral. The interlayer distance in Mt is approximately 12.45 Å (Cosultchi et al., 2004), which might instigate a diffusion process for contaminants in the nanocomposite adsorbent (Dąbrowski et al., 2005; Tanboonchuy et al., 2012).

The rate constants k_1 and k_2 of As^V adsorption on Mt were much greater than for NZVI and NZVI-Mt (Table 1), indicating that As^V could be removed by Mt through an ion exchange reaction (in exchange with -OH) on its surface (Li et al., 2017). From the PSO equation, we calculated the initial adsorption rate (h) (Wang et al., 2014; Arancibia-Miranda et al., 2016). The h for As^V in the mono-component system followed: NZVI < Mt < NZVI-Mt, but the presence of Se^{VI} changed the trend as: Mt < NZVI < NZVI-Mt (Table 1). Considering that h is associated to the sites that are available for the adsorption to occur, when $t \rightarrow 0$, it could be suggested that after the support of NZVI on Mt, there was a synergism in the adsorption as a result of the formation of new adsorption sites in NZVI-Mt giving greater specificity for As^V in contrast with NZVI (Zhang et al., 2005).

3.2.3. Isotherms of adsorption

The experimental adsorption isotherm data for of Se^{VI} and As^V onto Mt, NZVI and NZVI-Mt are summarized in Table S6, and their trend is shown in Fig. 6. In the mono-component system, adsorption isotherms of Se^{VI} were "*L*" type (Fig. 6a) (Dąbrowski et al., 2005; Limousin et al., 2007), indicating that there was a high affinity between the reactive surface groups of the adsorbent and adsorbate. The isotherms of As^V adsorption onto NZVI and NZVI-Mt (Fig. 6b and 6d) showed an "*H*" type isotherm, accounting for an extremely strong adsorption of the analyte (Dąbrowski et al., 2005; Boparai et al., 2011). Furthermore, the PC values for As^V on NZVI and NZVI-Mt in both systems, and for Se^{VI} in single-component system decreased with an increase of equilibrium adsorbate concentration (Table S7), following an exponential decrease until reaching a minimum value (Fig. S6). This trend could be attributed to the high affinity of the

adsorbents for both oxyanions at specific reaction sites at low adsorbate concentration (Basta and Tabatabai, 1992; Molina et al., 2010).

The Freundlich and Langmuir isotherm equations were used to describe the equilibrium adsorption data of oxyanions on the adsorbents (Table 2). A good description to the experimental data of Se^{VI} adsorption onto NZVI-Mt was obtained with the Freundlich equation ($r^2 = 0.944$ and $\chi^2 = 5.026$). These results suggested that the adsorption of Se^{VI} took place through forming multilayers on the heterogeneous surface of the adsorbing material. The values of r^2 for the adsorption of Se^{VI} on NZVI were quite similar between the equations used ($r^2 = 0.955$ and $\chi^2 = 0.562$ for Langmuir; and $r^2 = 0.957$ and $\chi^2 = 0.540$ for Freundlich) (Table 2). However, we must consider the theoretical foundation of the mathematical equations applied. So, knowing the oxidation process that NZVI underwent, as seen in the post-adsorption XRD investigation (Fig. 1c), it was unexpected that the adsorption sites present on the surface of the material would be similar or equal in energy and selectivity (Rangabhashiyam et al., 2014). Thus, the Freundlich equation explained the adsorption of Se^{VI} on the nanoparticles with heterogeneous surface sites better than the Langmuir equation.

The chemical reactivity of NZVI might induce Se^{VI} to be reduced to Se^{IV} (Qiu et al., 2000), a process that might occur on the adsorbent surface by adsorbing Se^{IV} on the outer shell Fe oxides of the NZVI (Yoon et al., 2011). The Se^{IV} (SeO_3^{2-}) adsorbed on the surface might also penetrate into the (oxy)hydroxide layers, and subsequently elemental selenium (Se^0) could be formed due to Se^{IV} reduction by NZVI (Hayashi et al., 2009). Another possibility might be that the adsorbed Se^{VI} would form multilayers on the adsorbent (Yoon et al., 2011; Xia et al., 2017a). However, future experiments are needed to prove the above hypotheses by investigating the solid phase

speciation of Se and/or Fe possibly using the method like x-ray photoelectron spectroscopy (XPS).

The experimental data of As^{V} also showed a high level of fitness with the Freundlich equation for all the studied adsorbents and systems (Table 2), and they agreed with the results reported previously (Kanel et al., 2005; Baltazar et al., 2014). The values of n (adsorption affinity) and PC for all the systems are summarized in Table 2. In the mono-component system, the value of n and PC for the elimination of Se^{VI} by NZVI-Mt was greater than that of NZVI (Table 2), indicating that the nanocomposite had a greater affinity for Se^{VI} compared to NZVI (Xia et al., 2017a).

In the case of As^{V}, the value of n varied between 3 and 6, and PC between 0.03 and 0.07 $mg \cdot g^{-1} \cdot \mu M^{-1}$, in both the mono-component and competitive systems, which indicated that the adsorption of this analyte was, by both adsorbents, a highly favorable process, and also suggesting that Se^{VI} did not interfere in the adsorption of As^{V}. This was confirmed from the fact that there was no big variation in the n and PC values in a competing system compared to the mono-component system (Table 2) (Guan et al., 2009; Liu et al., 2016).

4. Advantage of the use of NZVI-Mt in complex aqueous matrices

Pollution of aquatic environments with oxyanions (e.g., AsO_4^{3-}, SeO_4^{2-}, PO_4^{3-}, NO_3^{-}, and MnO_4^{-}) impacts the health of various communities around the world (Zhang et al., 2005; Wen et al., 2014), and it is a serious issue that needs to be solved. At present, the abatement of pollutants in aqueous matrices is achieved using high-cost techniques that are not easily accessible, and may generate toxic by-products (Singh et al., 2015; He et al., 2018). The use of nanotechnology, for example, NZVI-clay composite materials, has appeared as an excellent alternative for removing

oxyanions like Se^{VI} and As^{V} from water systems (Table 3). The NZVI-Mt nanocomposite reported in this study showed higher or at least comparable As^{V} and Se^{VI} removal capacities compared to nanocomposites on substrates such as activated carbon, carbon nanotubes (CNTs), graphite oxide (GO), zeolite and synthetic resin (Table 3). Adsorption capacity can vary depending on initial adsorbate concentrations and doses, and hence would not appropriately evaluate the real performance of an adsorbent which PC could do (Al-Wabel et al., 2019; Szulejko et al., 2019; Vikrant and Kim, 2019). The PC values for As^{V} and Se^{VI} removal using NZVI-Mt were smaller than those given by other adsorbents, except for As^{V} removal by zeolite (Suazo-Hernández et al., 2019) and pristine Mt (Bhowmick et al., 2014) (Table 3). These results could be attributed to high concentration of As^{V} and Se^{VI} that are not absorbed, making the adsorbent appear to have reduced performance. It is also probable that PC values depend on the NZVI immobilizing substrate which can interact differently with oxyanions (Liu and Hu, 2019; Vikrant and Kim, 2019). For instance, when NZVI was mixed with Al-bentonite, and an initial concentration of Se^{VI} was 80 $mg \cdot L^{-1}$, the PC was 18 times higher than for NZVI-Mt using 200 $mg \cdot L^{-1}$ of Se^{VI} (Table 3). Similarly, when NZVI was supported on graphite oxide (GO), and the initial concentration of As^{V} was 15 $mg \cdot L^{-1}$ (Zhu et al., 2009), PC was 9.9 times higher than NZVI-Mt at 200 $mg \cdot L^{-1}$ As^{V} concentration (Table 3). It is recommended that future research on As and Se removal in solid-liquid system should consider PC to evaluate adsorbent performance. Nevertheless, among the substrate materials, Mt would be less expensive and environmentally friendlier than CNT, GO and synthetic resins (Mandal et al., 2018; Mukhopadhyay et al., 2020). The present research made an exhaustive study of more complex matrices, finding that there was a greater removal of As^{V} in the system competing with Se^{VI} when using NZVI-Mt. This phenomenon showed the high affinity of NZVI-Mt for As^{V}, which might be attributed to the fact

that, as compared to the Se^{VI} species, As^{V} species present in the solution (pH = 7) had a spatial conformation (Fig. S4) that allowed forming more stable chemical bonds with less energy spending (Sherman and Randall, 2003). The chemical bond formation was facilitated with the ≡FeOH, ≡AlOH and ≡SiOH functional groups of the adsorbent material (Tandon et al., 2013). The consequence of using an expandable clay mineral such as montmorillonite to immobilize NZVI was that the laminar intercalation process taking place between the clay mineral and NZVI might favor the formation of additional removal sites due to the presence of NZVI. This paper also suggests that the contaminant adsorption studies must not only focus on the search for new nanomaterials that are efficient for the removal of pollutants in systems closer to reality but also should shed importance on determining the adsorbent-adsorbate interactions involved.

5. Conclusions

The characterization of NZVI-Mt and NZVI before and after the As^{V} and Se^{VI} adsorption reactions in both mono-component and competitive systems showed that the Fe^{0} nanoparticles grew in their particle size because they underwent a surface transformation process forming new mineralogical phases such as magnetite (Fe_3O_4) and/or maghemite (γ-Fe_2O_3), lepidocrocite (γ-FeOOH), and amorphous iron oxides. In the mono-component system, Se^{VI} was removed by the NZVI and NZVI-Mt more rapidly than As^{V}. In a competitive system, Se^{VI} was removed only by the NZVI, in contrast to As^{V} which was removed by all the adsorbents (Mt, NZVI, and NZVI-Mt). In addition, the kinetics of As^{V} adsorption onto NZVI and NZVI-Mt presented a better fit to the PSO equation ($r^2 > 0.98$, $\chi^2 < 1.50$), and giving q_e values 6.80 and 5.52 times greater, respectively, than Se^{VI} in the mono-component system.

The predominant mechanism of Se^{VI} removal from the solution by the adsorbents was through chemical adsorption. Meanwhile, in the mono-component and competing systems, As^{V} was removed by NZVI and NZVI-Mt forming monodentate or bidentate complexes. Higher q_{max} and PC values for As^{V} adsorption by NZVI-Mt in both systems and Se^{VI} adsorption in monocomponent system showed a synergistic effect due to NZVI immobilization on Mt, which also improved the affinity of NZVI-Mt toward As^{V} over Se^{VI}. This study showed promising results for applying Mt-supported NZVI to remove As^{V} coexisting with Se^{VI} in aqueous solutions. Future research is required to study the removal performance of oxyanions from real domestic and industrial wastewaters, and to investigate the nanocomposite stability.

Acknowledgements

This work was supported by FONDEF under Project no. ID17I10302, Fondecyt 1191018, PAI77190014, and by CEDENNA (FB0807). J.S.H acknowledges ANID Ph.D. scholarships Nº 21171685, and Convenio Marco Plurianual FRO1656.

References

Ahmed, E., Deep, A., Kwon, E.E., Brown, R.J.C., Kim, K.H., 2016. Performance comparison of MOF and other sorbent materials in removing key odorants emitted from pigpen slurry. Sci. Rep. 6, 1–11.

Al-Wabel, M., Elfaki, J., Usman, A., Hussain, Q., Ok, Y.S., 2019. Performance of dry water- and porous carbon-based sorbents for carbon dioxide capture. Environ. Res. 174, 69–79.

Arancibia-Miranda, N., Baltazar, S.E., García, A., Muñoz-Lira, D., Sepúlveda, P., Rubio, M.A., Altbir, D., 2016. Nanoscale zero valent supported by Zeolite and Montmorillonite:

Template effect of the removal of lead ion from an aqueous solution. J. Hazard. Mater. 301, 371–380.

Arancibia-miranda, N., Baltazar, S.E., García, A., Romero, A.H., Rubio, M.A., Altbir, D., 2014. Lead removal by nano-scale zero valent iron : Surface analysis and pH effect. Mater. Res. Bull. 59, 341–348.

Arancibia-Miranda, N., Escudey, M., Ramírez, R., González, R.I., Van Duin, A.C.T., Kiwi, M., 2017. Advancements in the Synthesis of Building Block Materials: Experimental Evidence and Modeled Interpretations of the Effect of Na and K on Imogolite Synthesis. J. Phys. Chem. C 121, 12658–12668.

Baikousi, M., Georgiou, Y., Daikopoulos, C., Bourlinos, A.B., Filip, J., Zbořil, R., Deligiannakis, Y., Karakassides, M.A., 2015. Synthesis and characterization of robust zero valent iron/mesoporous carbon composites and their applications in arsenic removal. Carbon N. Y. 93, 636–647.

Bajaj, M., Eiche, E., Neumann, T., Winter, J., Gallert, C., 2011. Concentrations of selenium in soil and groundwater in North-West India. J. Hazard. Mater. 189, 640–646.

Baltazar, S.E., Garcia, A., Romero, A.H., Rubio, M.A., Arancibia-Miranda, N., Altbir, D., 2014. Surface rearrangement of nanoscale zerovalent iron: the role of pH and its implications in the kinetics of arsenate sorption. Environ. Technol. (United Kingdom) 35, 2365–2372.

Barati, A.H., Maleki, A., Alasvand, M., 2010. Multi-trace elements level in drinking water and the prevalence of multi-chronic arsenical poisoning in residents in the west area of Iran. Sci. Total Environ. 408, 1523–1529.

Barkat, M., Nibou, D., Chegrouche, S., Mellah, A., 2009. Kinetics and thermodynamics studies of chromium(VI) ions adsorption onto activated carbon from aqueous solutions. Chem.

Eng. Process. Process Intensif. 48, 38–47.

Basta, N.T., Tabatabai, M.A., 1992. Effect of cropping systems on adsorption of metals by soils: III. Competitive adsorption. Soil Sci. 153, 195–204.

Bhowmick, S., Chakraborty, S., Mondal, P., Van Renterghem, W., Van den Berghe, S., Roman-Ross, G., Chatterjee, D., Iglesias, M., Renterghem, W. Van, 2014. Montmorillonite-supported nanoscale zero-valent iron for removal of arsenic from aqueous solution: Kinetics and mechanism. Chem. Eng. J. 243, 14–23.

Boparai, H.K., Joseph, M., Carroll, D.M.O., 2011. Kinetics and thermodynamics of cadmium ion removal by adsorption onto nano zerovalent iron particles. J. Hazard. Mater. 186, 458–465.

Chan, Y.T., Kuan, W.H., Chen, T.Y., Wang, M.K., 2009. Adsorption mechanism of selenate and selenite on the binary oxide systems. Water Res. 43, 4412–4420.

Charlet, L., Scheinost, A.C., Tournassat, C., Greneche, J.M., Géhin, A., Fernández-Martínez, A., Coudert, S., Tisserand, D., Brendle, J., 2007. Electron transfer at the mineral/water interface: Selenium reduction by ferrous iron sorbed on clay. Geochim. Cosmochim. Acta 71, 5731–5749.

Cosultchi, A., Bosch, P., Lara, V.H., 2004. Adsorption of petroleum organic compounds on natural Wyoming montmorillonite. Colloids Surfaces A Physicochem. Eng. Asp. 243, 53–61.

Dąbrowski, A., Podkościelny, P., Hubicki, Z., Barczak, M., 2005. Adsorption of phenolic compounds by activated carbon - A critical review. Chemosphere 58, 1049–1070.

Deng, Y., Ok, Y.S., Mohan, D., Pittman, C.U., Dou, X., 2019. Carbamazepine removal from water by carbon dot- modified magnetic carbon nanotubes. Environ. Res. 434–444.

El-Temsah, Y.S., Oughton, D.H., Joner, E.J., 2013. Effects of nano-sized zero-valent iron on DDT degradation and residual toxicity in soil: A column experiment. Plant Soil 368, 189–200.

Fan, Z., Zhang, Q., Gao, B., Li, M., Liu, C., Qiu, Y., 2019. Removal of hexavalent chromium by biochar supported nZVI composite: Batch and fixed-bed column evaluations, mechanisms, and secondary contamination prevention. Chemosphere 217, 85–94.

Fernández-Martínez, A., Charlet, L., 2009. Selenium environmental cycling and bioavailability: A structural chemist point of view. Rev. Environ. Sci. Biotechnol. 8, 81–110.

Guan, X., Dong, H., Ma, J., Jiang, L., 2009. Removal of arsenic from water: Effects of competing anions on As(III) removal in $KMnO_4$–Fe(II) process. Water Res. 43, 3891–3899.

Hayashi, H., Kanie, K., Shinoda, K., Muramatsu, A., Suzuki, S., Sasaki, H., 2009. pH-dependence of selenate removal from liquid phase by reductive Fe(II)-Fe(III) hydroxysulfate compound, green rust. Chemosphere 76, 638–643.

He, Y., Xiang, Y., Zhou, Y., Yang, Y., Zhang, J., Huang, H., 2018. Selenium contamination , consequences and remediation techniques in water and soils : A review. Environ. Res. 164, 288–301.

Hiemstra, T., Antelo, J., Rahnemaie, R., Riemsdijk, W.H. van, 2010. Nanoparticles in natural systems I: The effective reactive surface area of the natural oxide fraction in field samples. Geochim. Cosmochim. Acta 74, 41–58.

Hu, H.C., Chai, X.S., Barnes, D., 2014. Determination of solid-liquid partition coefficient of volatile compounds by solid phase ratio variation based headspace analysis. Fluid Phase Equilib. 380, 76–81.

Huq, S.M.I., Joardar, J.C., Parvin, S., Correll, R., Naidu, R., 2006. Arsenic Contamination in Food-chain : Transfer of Arsenic into Food Materials through Groundwater Irrigation 24, 305–316.

Impellitteri, C.A., 2004. Effects of pH and competing anions on the speciation of arsenic in fixed ionic strength solutions by solid phase extraction cartridges. Water Res. 38, 1207–14.

Jackson, B.P., Miller, W.P., 2000. Effectiveness of Phosphate and Hydroxide for Desorption of Arsenic and Selenium Species from Iron Oxides. Soil Sci. Soc. Am. J. 64, 1616–1622.

Jain, A., Agarwal, M., 2017. Kinetic equilibrium and thermodynamic study of arsenic removal from water using alumina supported iron nano particles. J. Water Process Eng. 19, 51–59.

Jain, R., Dominic, D., Jordan, N., Weiss, S., Hubner, R., van Hullebusch, E.D., Farges, F., Lens, P.N.L., 2015. Adsorption of copper and cadmium by biogenic elemental selenium nanoparticles. Chem. Eng. J. J. 260, 855–863.

Jia, Z., Shu, Y., Huang, R., Liu, J., Liu, L., 2018. Enhanced reactivity of nZVI embedded into supermacroporous cryogels for highly efficient Cr(VI) and total Cr removal from aqueous solution. Chemosphere 199, 232–242.

Kanel, S.R., Manning, B., Charlet, L., Choi, H., 2005. Removal of Arsenic(III) from Groundwater by Nanoscale Zero-Valent Iron. Environ. Sci. Technol. 39, 1291–1298.

Kim, K.H., Szulejko, J.E., Raza, N., Kumar, V., Vikrant, K., Tsang, D.C.W., Bolan, N.S., Ok, Y.S., Khan, A., 2019. Identifying the best materials for the removal of airborne toluene based on performance metrics - A critical review. J. Clean. Prod. 241, 118408.

Kim, S.A., Kamala-Kannan, S., Lee, K.J., Park, Y.J., Shea, P.J., Lee, W.H., Kim, H.M., Oh, B.T., 2013. Removal of Pb(II) from aqueous solution by a zeolite-nanoscale zero-valent iron composite. Chem. Eng. J. 217, 54–60.

Lee, J.S., Ko, YS, 2014. Synthesis of petaloid graphene/polyethylene composite nanosheet produced by ethylene polymerization with metallocene catalyst adsorbed on multilayer graphene. Catal. Today 232, 82–88.

Li, Y., Cheng, W., Sheng, G., Li, J., Dong, H., Chen, Y., Zhu, L., 2015. Synergetic effect of a pillared bentonite support on SE(VI) removal by nanoscale zero valent iron. Appl. Catal. B Environ. 174–175, 329–335.

Li, Z., Wang, L., Meng, J., Liu, X., Xu, J., Wang, F., Brookes, P., 2017. Zeolite-supported nanoscale zero-valent iron: New findings on simultaneous adsorption of Cd(II), Pb(II), and As(III) in aqueous solution and soil. J. Hazard. Mater. 344, 1–11.

Limousin, G., Gaudet, J.-P., Charlet, L., Szenknect, S., Barthès, V., Krimissa, M., 2007. Sorption isotherms: A review on physical bases, modeling and measurement. Appl. Geochemistry 22, 249–275.

Lin, J., Sun, M., Liu, X., Chen, Z., 2017. Functional kaolin supported nanoscale zero-valent iron as a Fenton-like catalyst for the degradation of Direct Black G. Chemosphere 184, 664–672.

Ling, L., Pan, B., Zhang, W. xian, 2015. Removal of selenium from water with nanoscale zero-valent iron: Mechanisms of intraparticle reduction of Se(IV). Water Res. 71, 274–281.

Liu, T., Yang, Y., Wang, Z.-L., Sun, Y., 2016. Remediation of arsenic(III) from aqueous solutions using improved nanoscale zero-valent iron on pumice. Chem. Eng. J. 288, 739–744.

Liu, Y., Hu, X., 2019. Kinetics and thermodynamics of efficient phosphorus removal by a composite fiber. Appl. Sci. 9, 2220–2239.

Luo, S., Qin, P., Shao, J., Peng, L., Zeng, Q., Gu, J.D., 2013. Synthesis of reactive nanoscale

zero valent iron using rectorite supports and its application for Orange II removal. Chem. Eng. J. 223, 1–7.

Luther, S., Borgfeld, N., Kim, J., Parsons, J.G., 2012. Removal of arsenic from aqueous solution : A study of the effects of pH and interfering ions using iron oxide nanomaterials. Microchem. J. 101, 30–36.

Mandal, S., Sarkar, B., Mukhopadhyay, R., Biswas, J.K., Manjaiah, K.M., 2018. Microparticle-Supported Nanocomposites for Safe Environmental Applications. Nanomater. Ecotoxicity, Safety, Public Percept. 305–317.

Martinson, C.A., Reddy, K.J., 2009. Adsorption of arsenic(III) and arsenic(V) by cupric oxide nanoparticles. J. Colloid Interface Sci. 336, 406–411.

Molina, M., Manquian-Cerda, K., Escudey, M., 2010. Sorption and selectivity sequences of Cd, Cu, Ni, Pb, and Zn in single- and multi-component systems in a cultivated chilean Mollisol. Soil Sediment Contam. 19, 405–418.

Mukhopadhyay, R., Bhaduri, D., Sarkar, B., Rusmin, R., Hou, D., Khanam, R., Sarkar, S., Kumar Biswas, J., Vithanage, M., Bhatnagar, A., Ok, Y.S., 2020. Clay–polymer nanocomposites: Progress and challenges for use in sustainable water treatment. J. Hazard. Mater. 383, 121125.

Na, C.-J., Yoo, M.-J., Tsang, D.C.W., Kim, H.W., Kim, K.-H., 2019. High-performance materials for effective sorptive removal of formaldehyde in air. J. Hazard. Mater. 366, 452–465.

Nazari, A.M., Radzinski, R., Ghahreman, A., 2017. Review of arsenic metallurgy: Treatment of arsenical minerals and the immobilization of arsenic. Hydrometallurgy 174, 258–281.

Neupane, G., Donahoe, R.J., Arai, Y., 2014. Kinetics of competitive

adsorption/desorption of arsenate and phosphate at the ferrihydrite-water interface. Chem. Geol. 368, 31–38.

O'Connor D.J. and Connolly J.P., 1980. The effect of concentration of adsorbing solids on the partition coefficient Water Research 14, 1517-1523.

Otyepka, M., 2014. Challenges in the Theoretical Description of Nanoparticle Reactivity : Nano Zero-Valent Iron. Int J Quantum Chem. 114, 987–992.

Pang, Z., Yan, M., Jia, X., Wang, Z., Chen, J., 2014. Debromination of decabromodiphenyl ether by organo-montmorillonite- supported nanoscale zero-valent iron : Preparation , characterization and influence factors. J. Environ. Sci. 26, 483–491.

Peak, D., 2006. Adsorption mechanisms of selenium oxyanions at the aluminum oxide/water interface. J. Colloid Interface Sci. 303, 337–345.

Peng, Z., Xiong, C., Wang, W., Tan, F., Xu, Y., Wang, X., Qiao, X., 2017. Facile modification of nanoscale zero-valent iron with high stability for Cr(VI) remediation. Sci. Total Environ. 596–597, 266–273.

Prasanth, R., Shubha, N., Hng, H.H., Srinivasan, M., 2013. Effect of nano-clay on ionic conductivity and electrochemical properties of poly(vinylidene fluoride) based nanocomposite porous polymer membranes and their application as polymer electrolyte in lithium ion batteries. Eur. Polym. J. 49, 307–318.

Qiu, S.R., Lai, H.F., Roberson, M.J., Hunt, M.L., Amrhein, C., Giancarlo, L.C., Flynn, G.W., Yarmoff, J.A., 2000. Removal of contaminants from aqueous solution by reaction with iron surfaces. Langmuir 16, 2230–2236.

Rangabhashiyam, S., Anu, N., Giri Nandagopal, M.S., Selvaraju, N., 2014. Relevance of isotherm models in biosorption of pollutants by agricultural byproducts. J. Environ.

Chem. Eng. 2, 398–414.

Rovira, M., Giménez, J., Martínez, M., Martínez-Lladó, X., de Pablo, J., Martí, V., Duro, L., 2008. Sorption of selenium(IV) and selenium(VI) onto natural iron oxides: Goethite and hematite. J. Hazard. Mater. 150, 279–284.

Santos, S., Ungureanu, G., Boaventura, R., Botelho, C., 2015. Selenium contaminated waters: An overview of analytical methods, treatment options and recent advances in sorption methods. Sci. Total Environ. 521–522, 246–260.

Sheng, G., Alsaedi, A., Shammakh, W., Monaquel, S., Sheng, J., Wang, X., Li, H., Huang, Y., 2016. Enhanced sequestration of selenite in water by nanoscale zero valent iron immobilization on carbon nanotubes by a combined batch, XPS and XAFS investigation. Carbon N. Y. 99, 123–130.

Sherman, D.M., Randall, S.R., 2003. Surface complexation of arsenic(V) to iron(III) (hydr)oxides: Structural mechanism from ab initio molecular geometries and EXAFS spectroscopy. Geochim. Cosmochim. Acta 67, 4223–4230.

Singh, R., Singh, S., Parihar, P., Singh, V.P., Prasad, S.M., 2015. Arsenic contamination, consequences and remediation techniques: A review. Ecotoxicol. Environ. Saf. 112, 247–270.

Suazo-Hernández, J., Sepúlveda, P., Manquián-Cerda, K., Ramírez-Tagle, R., Rubio, M.A., Bolan, N., Sarkar, B., Arancibia-Miranda, N., 2019. Synthesis and characterization of zeolite-based composites functionalized with nanoscale zero-valent iron for removing arsenic in the presence of selenium from water. J. Hazard. Mater. 373, 810–819.

Sun, F., Osseo-asare, K.A., Chen, Y., Dempsey, B.A., 2011. Reduction of As (V) to As (III) by commercial ZVI or As (0) with acid-treated ZVI. J. Hazard. Mater. 196, 311–317.

Sun, Y., Ding, C., Cheng, W., Wang, X., 2014. Simultaneous adsorption and reduction of U(VI) on reduced graphene oxide-supported nanoscale zerovalent iron. J. Hazard. Mater. 280, 399–408.

Szulejko, J.E., Kim, K., Parise, J., 2019. Seeking the most powerful and practical real-world sorbents for gaseous ben- zene as a representative volatile organic compound based on performance metric. Sep. Purif. Technol. 212, 980–985.

Tanboonchuy, V., Grisdanurak, N., Liao, C.H., 2012. Background species effect on aqueous arsenic removal by nano zero-valent iron using fractional factorial design. J. Hazard. Mater. 205–206, 40–46.

Tandon, P.K., Shukla, R.C., Singh, S.B., 2013. Removal of arsenic (III) from water with clay supported zero valent iron nanoparticles synthesized with the help of tea liquor. Ind. Eng. Chem. Res. 52, 10052–10058.

Tofighy, M.A., Mohammadi, T., 2011. Adsorption of divalent heavy metal ions from water using carbon nanotube sheets. J. Hazard. Mater. 185, 140–147.

Trujillo-Reyes, J., Peralta-Videa, J.R., Gardea-Torresdey, J.L., 2014. Supported and unsupported nanomaterials for water and soil remediation : Are they a useful solution for worldwide pollution ? J. Hazard. Mater. 280, 487–503.

~~Violante, A., Pigna, M., 2010. Competitive Sorption of Arsenate and Phosphate on Different Clay Minerals and Soils. Soil Sci. Soc. Am. J. 66, 1788.~~

Vikrant, K., Kim, K., 2019. Nanomaterials for the adsorptive treatment of Hg(II) ions from water. Chem. Eng. J. 358, 264–282.

Wang, C.-B., Zhang, W.-X., 1997. Synthesizing Nanoscale Iron Particles for Rapid and Complete Dechlorination of TCE and PCBs. Environ. Sci. Technol. 31, 2155–2156.

Wang, C., Luo, H., Zhang, Z., Wu, Y., Zhang, J., Chen, S., 2014. Removal of As(III) and As(V) from aqueous solutions using nanoscale zero valent iron-reduced graphite oxide modified composites. J. Hazard. Mater. 268, 124–131.

Wen, Z., Zhang, Y., Dai, C., 2014. Removal of phosphate from aqueous solution using nanoscale zerovalent iron (nZVI). Colloids Surfaces A Physicochem. Eng. Asp. 457, 433–440.

Wilkin, R.T., Lee, T.R., Beak, D.G., Anderson, R., Burns, B., 2018. Groundwater co-contaminant behavior of arsenic and selenium at a lead and zinc smelting facility. Appl. Geochemistry 89, 255–264.

Xi, Y., Sun, Z., Hreid, T., Ayoko, G.A., Frost, R.L., 2014. Bisphenol A degradation enhanced by air bubbles via advanced oxidation using in situ generated ferrous ions from nano zero-valent iron/palygorskite composite materials. Chem. Eng. J. 247, 66–74.

Xia, X., Ling, L., Zhang, W., 2017a. Genesis of pure Se(0) nano- and micro-structures in wastewater with nanoscale zero-valent iron (nZVI). Environ. Sci. Nano 4, 52–59.

Xia, X., Ling, L., Zhang, W. xian, 2017b. Solution and surface chemistry of the Se(IV)-Fe(0) reactions: Effect of initial solution pH. Chemosphere 168, 1597–1603.

Xie, W., Liang, Q., Qian, T., Zhao, D., 2015. Immobilization of selenite in soil and groundwater using stabilized Fe-Mn binary oxide nanoparticles. Water Res. 70, 485–494.

Xie, Y., Dong, H., Zeng, G., Zhang, L., Cheng, Y., 2017. The comparison of Se (IV) and Se (VI) sequestration by nanoscale zero-valent iron in aqueous solutions :The roles of solution chemistry. J. Hazard. Mater. 338, 306–312.

Yan, W., Ramos, M. a V, Koel, B.E., Zhang, W.X., 2012. As(III) sequestration by iron nanoparticles: Study of solid-phase redox transformations with X-ray photoelectron spectroscopy. J. Phys. Chem. C 116, 5303–5311.

Yoon, I.H., Kim, K.W., Bang, S., Kim, M.G., 2011. Reduction and adsorption mechanisms of selenate by zero-valent iron and related iron corrosion. Appl. Catal. B Environ. 104, 185–192.

Yuan, P., Fan, M., Yang, D., He, H., Liu, D., Yuan, A., Zhu, J., Chen, T., 2009. Montmorillonite-supported magnetite nanoparticles for the removal of hexavalent chromium [Cr(VI)] from aqueous solutions. J. Hazard. Mater. 166, 821–829.

Yucelen, G.I., Kang, D.Y., Guerrero-Ferreira, R.C., Wright, E.R., Beckham, H.W., Nair, S., 2012. Shaping single-walled metal oxide nanotubes from precursors of controlled curvature. Nano Lett. 12, 827–832.

Zhang, Y., Amrhein, C., Frankenberger, W.T., 2005. Effect of arsenate and molybdate on removal of selenate from an aqueous solution by zero-valent iron. Sci. Total Environ. 350, 1–11.

Zhang, Y., Li, Y., Dai, C., Zhou, X., Zhang, W., 2014. Sequestration of Cd(II) with nanoscale zero-valent iron (nZVI): Characterization and test in a two-stage system. Chem. Eng. J. 244, 218–226.

Zhang, Y., Li, Y., Li, J., Hu, L., Zheng, X., 2011. Enhanced removal of nitrate by a novel composite: Nanoscale zero valent iron supported on pillared clay. Chem. Eng. J. 171, 526–531.

Zhu, H., Jia, Y., Wu, X., Wang, H., 2009. Removal of arsenic from water by supported nano zero-valent iron on activated carbon. J. Hazard. Mater. 172, 1591–1596.

Zhu, J., Johnson, T.M., Finkelman, R.B., Zheng, B. shan, Sýkorová, I., Pešek, J., 2012. The occurrence and origin of selenium minerals in Se-rich stone coals, spoils and their adjacent soils in Yutangba, China. Chem. Geol. 330–331, 27–38.

Zhu, R., Chen, Q., Zhou, Q., Xi, Y., Zhu, J., He, H., 2015. Adsorbents based on montmorillonite for contaminant removal from water: A review. Appl. Clay Sci. 123, 239–258.

Figure Captions

Fig. 1. XRD patterns of (a) NZVI, (b) NZVI-Mt,(c) Se^{VI} / NZVI, (d) Se^{VI} / NZVI-Mt, (e) As^{V} / NZVI, (f) As^{V} / NZVI-Mt, (g) Se^{VI} - As^{V} / NZVI, and (h) Se^{VI} - As^{V} / NZVI-Mt after shaking with aqueous solution containing 200 $mg \cdot L^{-1}$ Se^{VI} and As^{V}.

Fig. 2. SEM images of (a) NZVI, (b) NZVI-Mt,(c) Se^{VI} / NZVI, (d) Se^{VI} / NZVI-Mt, (e) As^{V} / NZVI, (f) As^{V} / NZVI-Mt, (g) Se^{VI} - As^{V} / NZVI, and (h) Se^{VI} - As^{V} / NZVI-Mt

Fig. 3. Effect of pH on the adsorption of (a) only Se^{VI}, (b) only As^{V}, (c) Se^{VI} - As^{V}, and (d) As^{V} - Se^{VI} on Mt, NZVI and NZVI-Mt.

Fig. 4. ΔpH value for the adsorption of (a) only Se^{VI}, (b) only As^{V}, and (c) Se^{VI} - As^{V} on Mt, NZVI and NZVI**.**

Fig. 5. Pseudo-first-order and pseudo-second-order kinetics for the adsorption of (a) only Se^{VI}, (b) only As^{V}, (c) Se^{VI} - As^{V}, and (d) As^{V} - Se^{VI} on Mt, NZVI and NZVI-Mt.

Fig. 6. Langmuir and Freundlich isotherms for the adsorption of (a) only Se^{VI}, (b) only As^{V}, (c) Se^{VI} - As^{V}, and (d) As^{V} - Se^{VI} on Mt, NZVI and NZVI-Mt.

Table Captions

Table 1 Theoretically determined parameters with standard deviation of pseudo-first-order and pseudo-second-order kinetic equations for Se^{VI} and As^{V} adsorption on Mt, NZVI and NZVI-Mt in mono-component and competitive systems.

Table 2 Parameters with standard deviation of Langmuir and Freundlich isotherm models for Se^{VI} and As^{V} adsorption on NZVI and NZVI-Mt in mono-component and competitive systems.

Table 3 Performance of NZVI supported on different substrates for adsorption of As and Se from aqueous solution.

Figures

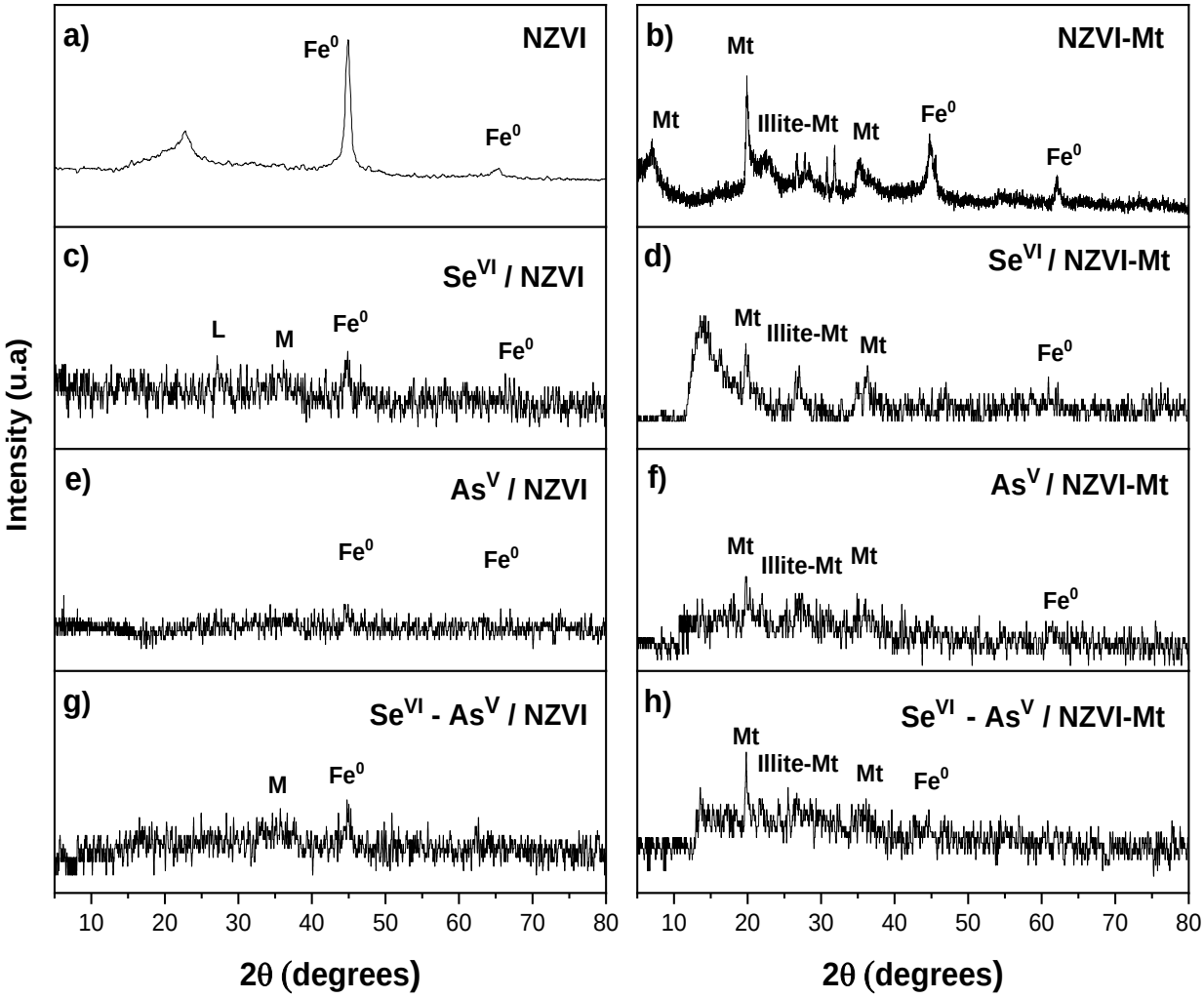

Fig. 1.

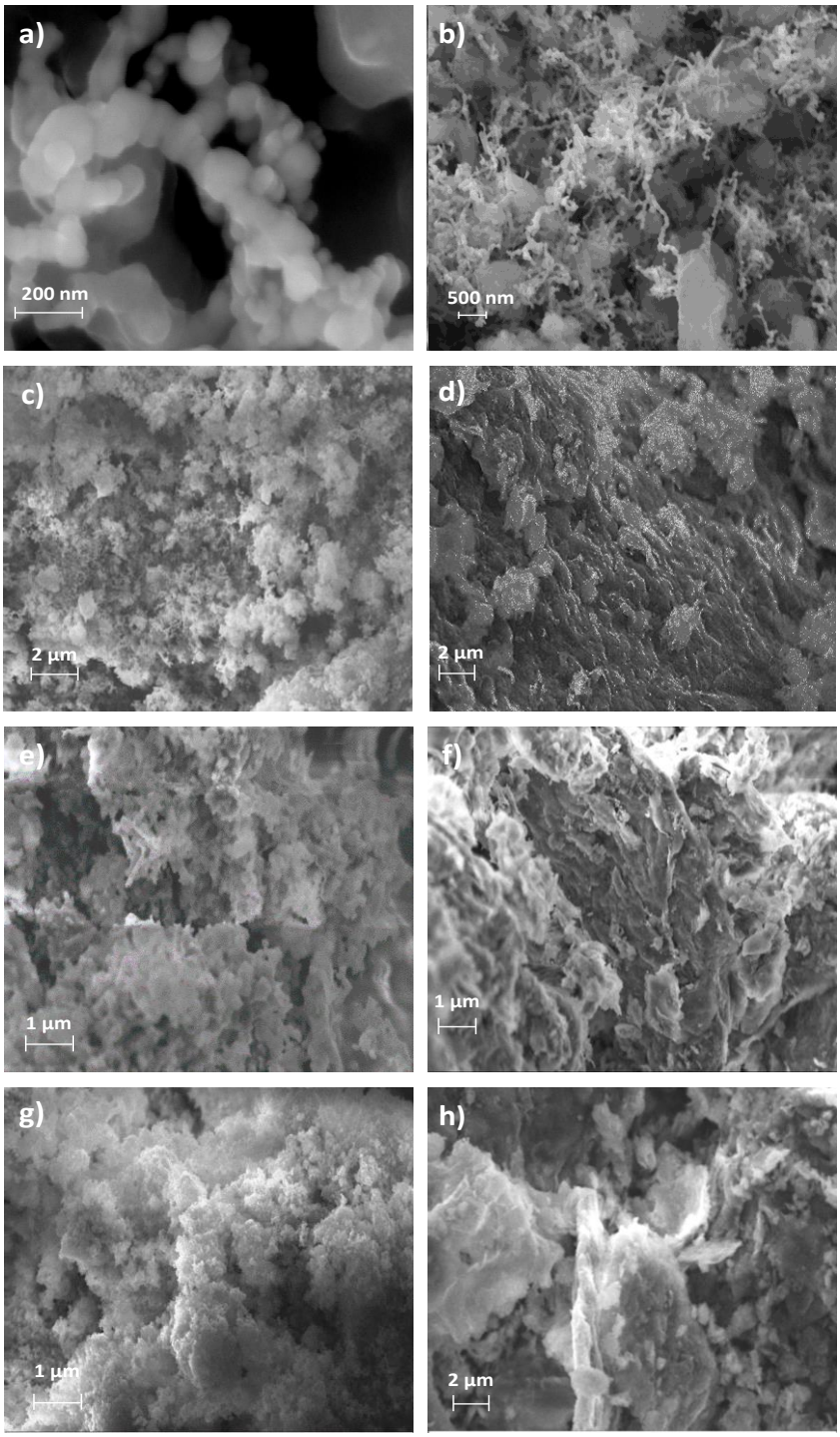

Fig. 2.

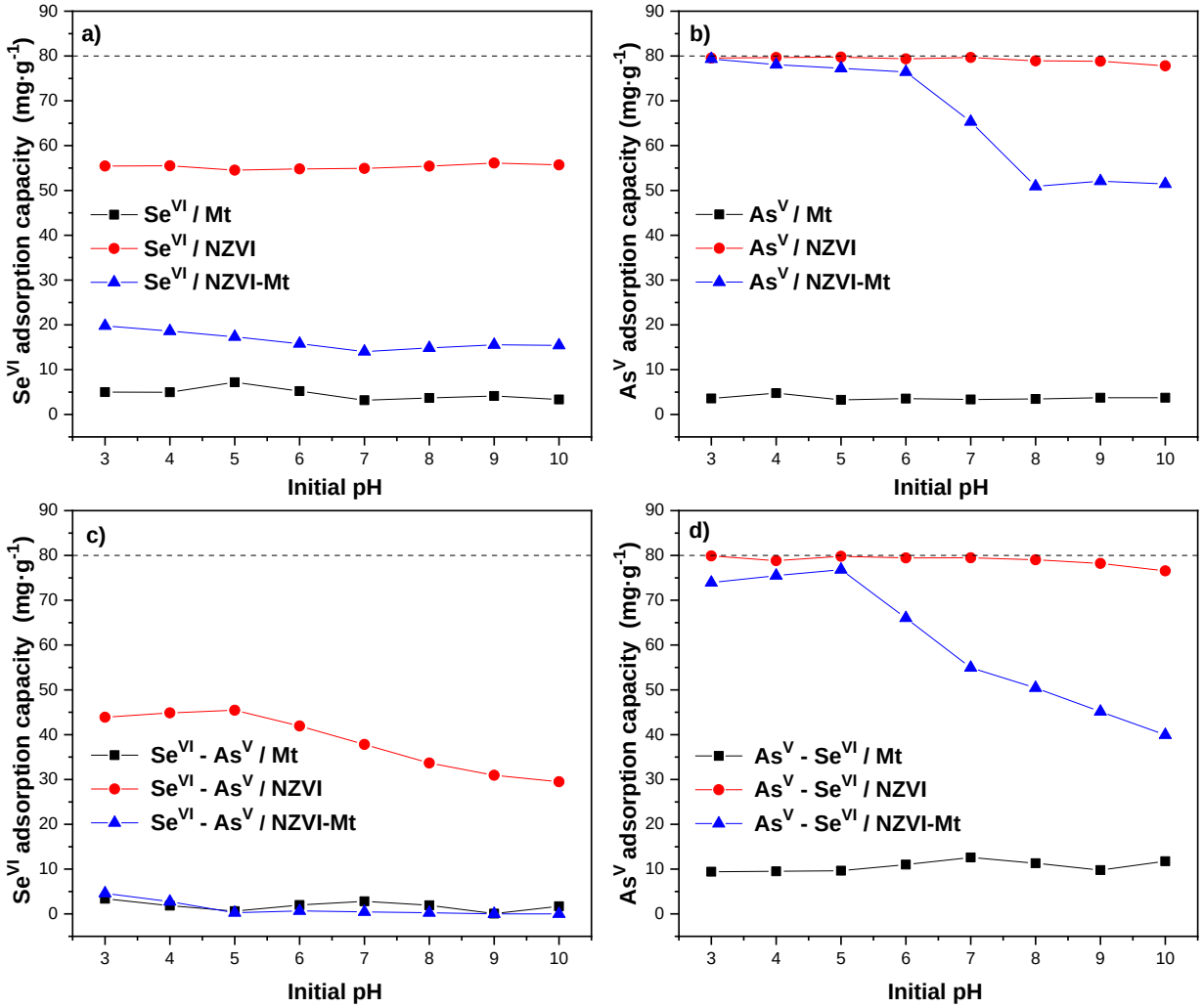
a)
b)
c)
d)
Se^VI adsorption capacity (mg·g^-1)
As^V adsorption capacity (mg·g^-1)
Initial pH
Se^VI / Mt
Se^VI / NZVI
Se^VI / NZVI-Mt
As^V / Mt
As^V / NZVI
As^V / NZVI-Mt
Se^VI - As^V / Mt
Se^VI - As^V / NZVI
Se^VI - As^V / NZVI-Mt
As^V - Se^VI / Mt
As^V - Se^VI / NZVI
As^V - Se^VI / NZVI-Mt

Fig. 3.

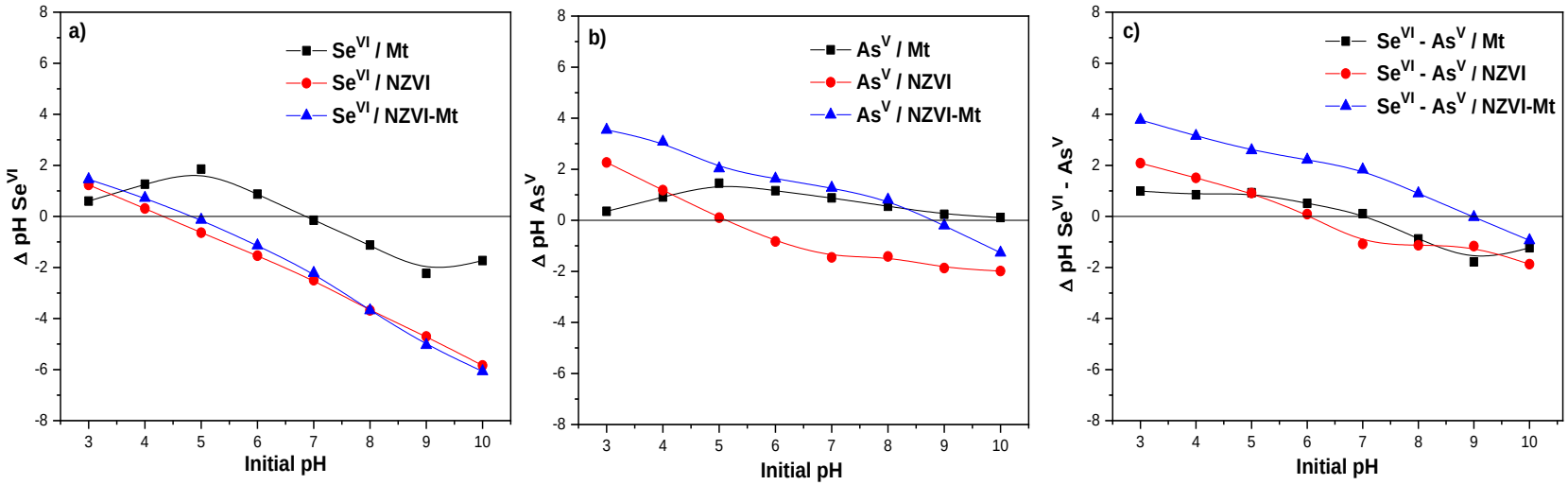
a)
Se^VI / Mt
Se^VI / NZVI
Se^VI / NZVI-Mt
Δ pH Se^VI
Initial pH
b)
As^V / Mt
As^V / NZVI
As^V / NZVI-Mt
Δ pH As^V
Initial pH
c)
Se^VI - As^V / Mt
Se^VI - As^V / NZVI
Se^VI - As^V / NZVI-Mt
Δ pH Se^VI - As^V
Initial pH

Fig. 4.

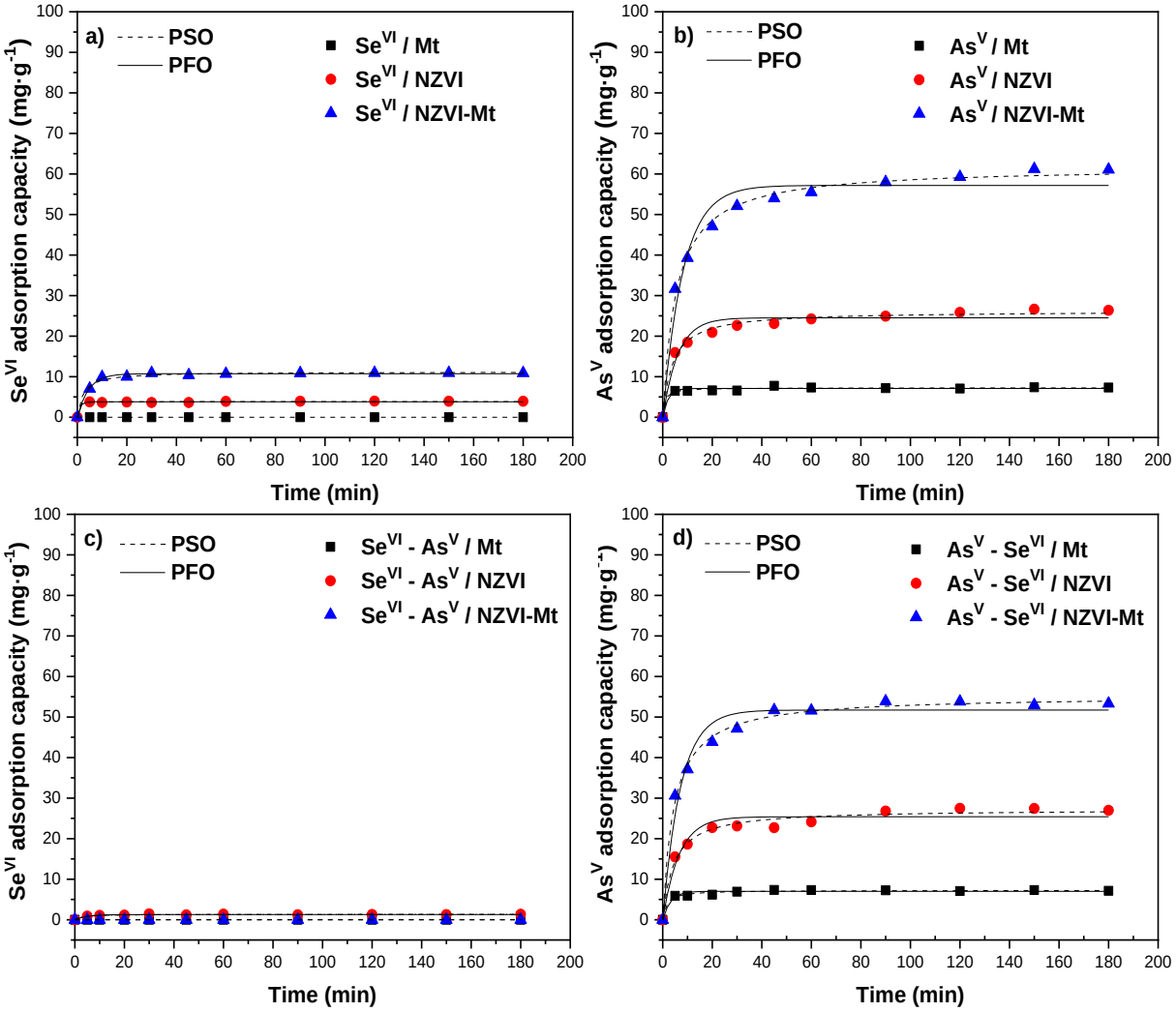
a)
PSO
PFO
Se^VI / Mt
Se^VI / NZVI
Se^VI / NZVI-Mt
Se^VI adsorption capacity (mg·g^-1)
Time (min)
b)
PSO
PFO
As^V / Mt
As^V / NZVI
As^V / NZVI-Mt
As^V adsorption capacity (mg·g^-1)
Time (min)
c)
PSO
PFO
Se^VI - As^V / Mt
Se^VI - As^V / NZVI
Se^VI - As^V / NZVI-Mt
Se^VI adsorption capacity (mg·g^-1)
Time (min)
d)
PSO
PFO
As^V - Se^VI / Mt
As^V - Se^VI / NZVI
As^V - Se^VI / NZVI-Mt
As^V adsorption capacity (mg·g^-1)
Time (min)

Fig. 5.

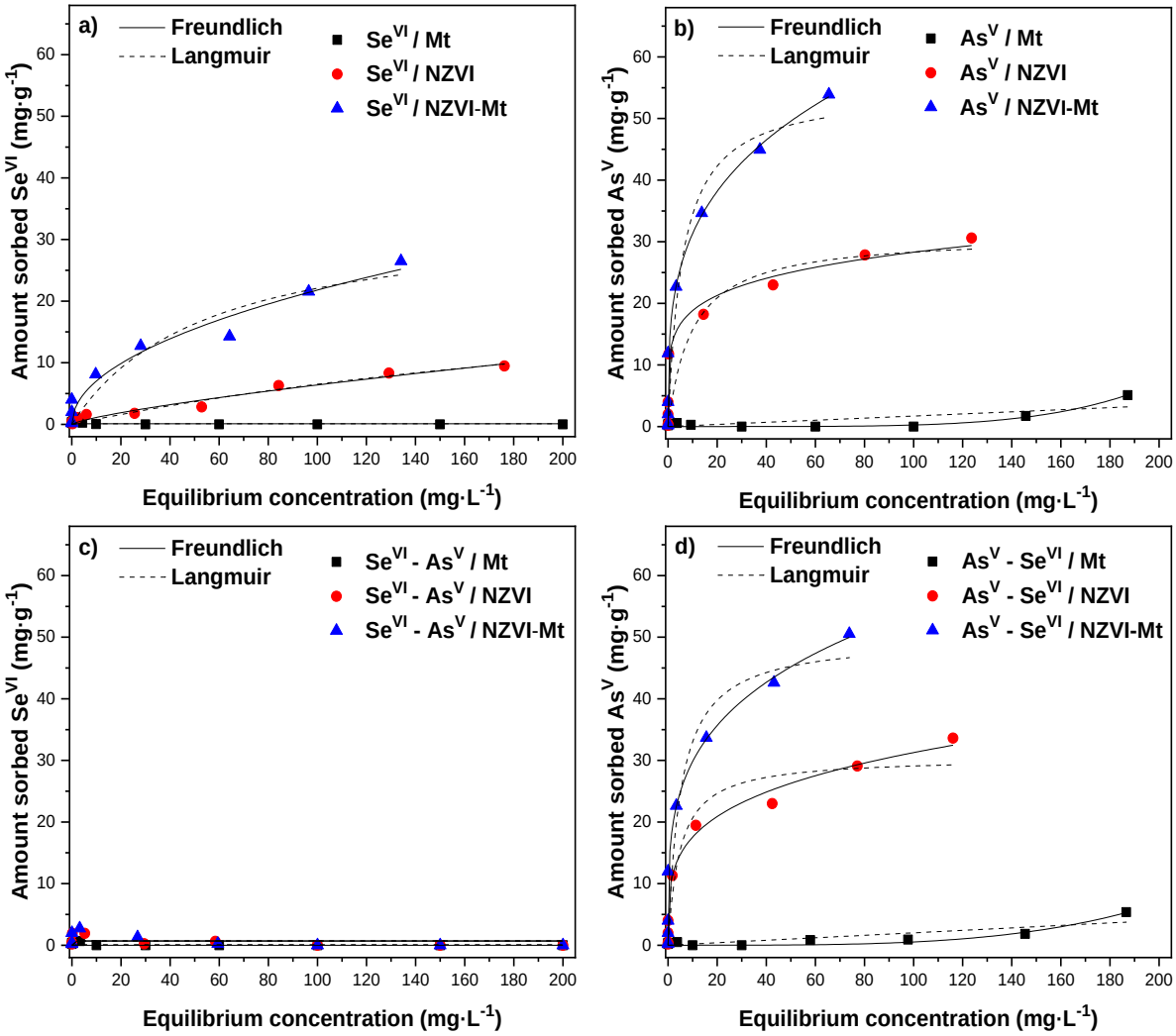
a)
Freundlich
Langmuir
Se^VI / Mt
Se^VI / NZVI
Se^VI / NZVI-Mt
Amount sorbed Se^VI (mg·g^-1)
Equilibrium concentration (mg·L^-1)
b)
Freundlich
Langmuir
As^V / Mt
As^V / NZVI
As^V / NZVI-Mt
Amount sorbed As^V (mg·g^-1)
Equilibrium concentration (mg·L^-1)
c)
Freundlich
Langmuir
Se^VI - As^V / Mt
Se^VI - As^V / NZVI
Se^VI - As^V / NZVI-Mt
Amount sorbed Se^VI (mg·g^-1)
Equilibrium concentration (mg·L^-1)
d)
Freundlich
Langmuir
As^V - Se^VI / Mt
As^V - Se^VI / NZVI
As^V - Se^VI / NZVI-Mt
Amount sorbed As^V (mg·g^-1)
Equilibrium concentration (mg·L^-1)

Fig. 6.

Tables

Table 1 Theoretically determined parameters with standard deviation of pseudo-first-order and pseudo-second-order kinetic equations for Se^{VI} and As^{V} adsorption on Mt, NZVI and NZVI-Mt in mono-component and competitive systems.

Kinetics parameters	**Se^{VI} Mono-component system**			**Se^{VI} Competitive system**		
	Mt	**NZVI**	**NZVI-Mt**	**Mt**	**NZVI**	**NZVI-Mt**
q_e,exp ($mg \cdot g^{-1}$)	0.00 ± 0.00	3.94 ± 0.64	10.88 ± 0.45	0.00 ± 0.00	1.33 ± 0.83	0.00 ± 0.00
q_e,exp (%)	0.00	4.92	13.61	0.00	1.67	0.00
Pseudo-first-order						
q,cal ($mg \cdot g^{-1}$)	N.D.	3.80 ± 0.05	10.73 ± 0.11	N.D.	1.27 ± 0.03	N.D.
k_1 (x 10^{-3} min^{-1})	N.D.	937.35 ± 177.04	221.43 ± 15.15	N.D.	205.60 ± 35.78	N.D.
r^2	N.D.	0.984	0.992	N.D.	0.945	N.D.
χ^2	N.D.	0.020	0.089	N.D.	0.009	N.D.
Pseudo-second-order						
q_e,cal ($mg \cdot g^{-1}$)	N.D.	3.85 ± 0.05	11.17 ± 0.18	N.D.	1.32 ± 0.04	N.D.
k_2 (x 10^{-3} $g \cdot mg^{-1} \cdot min^{-1}$)	N.D.	958.59 ± 99.71	38.89 ± 6.55	N.D.	310.82 ± 30.81	N.D.
h ($mg \cdot g^{-1} \cdot min^{-1}$)	N.D.	14.21 ± 0.00	4.85 ± 0.00	N.D.	0.54 ± 0.00	N.D.

r^2	N.D.	0.987	0.986	N.D.	0.946	N.D.
χ^2	N.D.	0.156	0.154	N.D.	0.008	N.D.
Kinetics parameters	**As^V Mono-component system**			**As^V Competitive system**		
	Mt	**NZVI**	**NZVI-Mt**	**Mt**	**NZVI**	**NZVI-Mt**
q_e,exp (mg·g^{-1})	7.28 ± 0.11	26.36 ± 0.77	61.08 ± 0.45	7.13 ± 0.43	26.97 ± 0.23	53.51 ± 0.91
q_e,exp (%)	9.14	32.93	76.31	8.95	33.69	66.64
Pseudo-first-order						
q_e,cal (mg·g^{-1})	7.09 ± 0.13	24.50 ± 0.66	57.17 ± 1.40	6.97 ± 0.15	25.39 ± 0.72	51.71 ± 1.09
k_1 (x 10^{-3} min^{-1})	461.36 ± 107.33	163.69 ± 26.40	121.80 ± 16.06	313.79- ± 59.57	151.34 ± 24.81	138.96 ± 12.46
r^2	0.967	0.946	0.960	0.958	0.943	0.968
χ^2	0.155	0.187	13.20	0.155	3.680	8.277
Pseudo-second-order						
q_e,cal (mg·g^{-1})	7.26 ± 0.14	26.18 ± 0.41	61.74 ± 0.64	7.23 ± 0.12	27.26 ± 0.55	55.25 ± 0.55
k_2 (x 10^{-3} g·mg^{-1}·min^{-1})	170.98 ± 18.43	9.76 ± 1.23	2.98 ± 0.22	89.07 ± 10.57	8.40 ± 1.31	4.05 ± 0.31
h (mg·g^{-1}·min^{-1})	9.01 ± 0.00	6.69 ± 0.00	11.36 ± 0.00	4.66 ± 0.00	6.24 ± 0.00	12.36 ± 0.00
r^2	0.977	0.988	0.996	0.984	0.981	0.996

χ^2	0.104	0.684	1.494	0.074	1.201	1.181

N.D.: Not determined.

Table 2 Parameters with standard deviation of Langmuir and Freundlich isotherm models for Se^{VI} and As^{V} adsorption on NZVI and NZVI-Mt in mono-component and competitive systems.

Sample	Langmuir constant				Freundlich constant				Partition coefficient
	K_L (x 10^{-3} L·mg^{-1})	q_{max} (mg·g^{-1})	r^2	χ^2	K_F ((mg·g^{1})(L·mg^{-1})$^{1/n}$)	n	r^2	χ^2	(mg·g^{-1}·μM^{-1})
Se^{VI} Mono-component system									
NZVI	2.94 ± 1.11	28.63 ± 4.85	0.955	0.562	0.19 ± 0.10	1.32 ± 0.19	0.957	0.540	0.021
NZVI-Mt	18.21 ± 10.34	34.21 ± 7.94	0.917	7.539	2.26 ± 0.97	2.03 ± 0.40	0.944	5.026	0.024
As^{V} Mono-component system									
NZVI	102. 41 ± 26.91	31.08 ± 4.97	0.857	21.143	12.51 ± 1.66	5.64 ± 1.04	0.970	4.368	0.034
NZVI-Mt	169.33 ± 10.17	54.75 ± 5.94	0.931	29.288	16.25 ± 3.97	3.51 ± 0.84	0.946	23.229	0.065
As^{V} Competitive system									
NZVI	210.70 ± 19.06	30.47 ± 2.45	0.937	10.504	9.85 ± 1.48	3.99 ± 0.58	0.976	4.058	0.033
NZVI-Mt	195.52 ± 15.90	49.91 ± 5.31	0.922	29.433	16.46 ± 4.19	3.87 ± 1.04	0.938	23.550	0.055

Table 3 Performance of NZVI supported on different substrates for adsorption of As and Se from aqueous solution.

Element	Substrate	Adsorption condition (ºT, pH)	Initial concentration ($mg \cdot L^{-1}$)	Initial concentration (µM)	Removal efficiency (%)	q_{max} ($mg \cdot g^{-1}$)	PC ($mg \cdot g^{-1} \cdot \mu M^{-1}$)*	BET-surface area ($m^2 \cdot g^{-1}$)	Reference
As^{V}	Zeolite	25, 7	200	2669.5	47.8	38.26	0.027	198.7	(Suazo-Hernández et al., 2019)
As^{III}	Zeolite	25, 6	10	133.5	62.2	12.84	0.269	–	(Li et al., 2018)
As^{III}	Montmorillonite	22,7	345	4604.9	22.4	59.9	0.017	36.97	(Bhowmick et al., 2014)
As^{V}			200	2669.5	28.6	45.5	0.024		
As^{III}	Graphite oxide	25, 7	15	200.2	95.5	35.83	3.98	100.65	(Wang et al., 2014)
As^{V}			15	200.2	77.4	29.04	0.642		

As^{III}	Alumina	50, 7	10	133.5	99.98	15.5	580.63	–	(Jain and Agarwal, 2017)
As^{III}	Activated carbon	25, 6.5	2	26.7	–	18.2	–	69.4	(Zhu et al., 2009)
As^{V}			2	26.7	–	12.0	–	–	
As^{III}	Starbon 300	- ,7	5.5	73.5	24.3	26.8	0.482	141	(Baikousi et al., 2015)
As^{III}	Chitosan-pumice	15, 6.2	100	1334.8	99.5	242.80	36.38	38.2	(Liu et al., 2016)
As^{V}	Montmorrillonite	25, 7	200	2669.5	68.43	54.75	0.065	209.0	This study
Se^{VI}	Al-bentonite	25, 6	80	1013.2	95.7	19.14	0.439	–	(Li et al., 2015)
Se^{IV}	Carbon nanotubes	25, 6	–	–	95.7	12.2	–	61.1	(Sheng et al., 2016)
Se^{VI}	Montmorillonite	25, 7	200	2532.9	42.76	34.21	0.024	209.0	This study

827

$$* \text{ Partition coefficient } = \frac{\text{Adsorption capacity}}{\text{Initial concentration x } (1 - \text{removal rate})} \text{ (Deng et al., 2019)}$$

Supporting Information

Efficient and selective removal of Se^{VI} and As^{V} mixed contaminants from aqueous media by montmorillonite-nanoscale zero valent iron nanocomposite

Jonathan Suazo-Hernández[a,b], Karen Manquián-Cerda[c], María de la Luz Mora[b,d], Mauricio Molina-Roco[e], María Angélica Rubio[c,f], Binoy Sarkar[g]*, Nanthi Bolan[h], Nicolás Arancibia-Miranda[c,f]*

[a]Programa de Doctorado en Ciencias de Recursos Naturales Universidad de La Frontera, Av. Francisco Salazar 01145, P.O. Box 54-D, Temuco, Chile

[b]Center of Plant, Soil Interaction and Natural Resources Biotechnology, Universidad de La Frontera. UFRO. Temuco, 4780000, Chile

[c]Facultad de Química y Biología, Universidad de Santiago de Chile, Av. B. O'Higgins, 3363, Santiago, Chile

[d]Departamento de Ciencias Químicas y Recursos Naturales, Universidad de La Frontera, Av. Francisco Salazar 01145, P.O. Box 54-D, Temuco, Chile

[e]Escuela de Agronomía, Universidad Mayor, Camino La Pirámide #5750, Huechuraba, Santiago 8580745, Chile

[f]Center for the Development of Nanoscience and Nanotechnology, CEDENNA, 9170124, Santiago, Chile

[g]Lancaster Environment Centre, Lancaster University, Lancaster, LA1 4YQ, UK

[h]Global Centre for Environmental Remediation, University of Newcastle, Callaghan, NSW 2308, Australia

* Co-corresponding authors:

Dr Binoy Sarkar; Lancaster University; e-mail: b.sarkar@lancaster.ac.uk

Dr Nicolás Arancibia-Miranda; Universidad de Santiago de Chile; e-mail: nicolas.arancibia@usach.cl

Analysis of data

The data were adjusted to kinetic mathematical equations and sorption isotherm equations, which were evaluated through the coefficient of determination (r^2) and Chi-square (χ^2) values. The χ^2 test measures the difference between the experimental and equations data, and is mathematically expressed by Eq. 1.

$$\chi^2 = \sum_{i=1}^{N} \frac{(q_e, \exp - q_e, \mathrm{cal})^2}{q_e, \mathrm{cal}} \qquad \text{(Eq .1)}$$

where, q_e, exp corresponds to the amount of solute adsorbed in the experimental data at equilibrium, and q_e, cal is the quantity adsorbed at equilibrium through the model. A smaller value of χ^2 indicates a better fit of the experimental data to the equations (Arancibia-Miranda et al., 2016; Boparai et al., 2011).

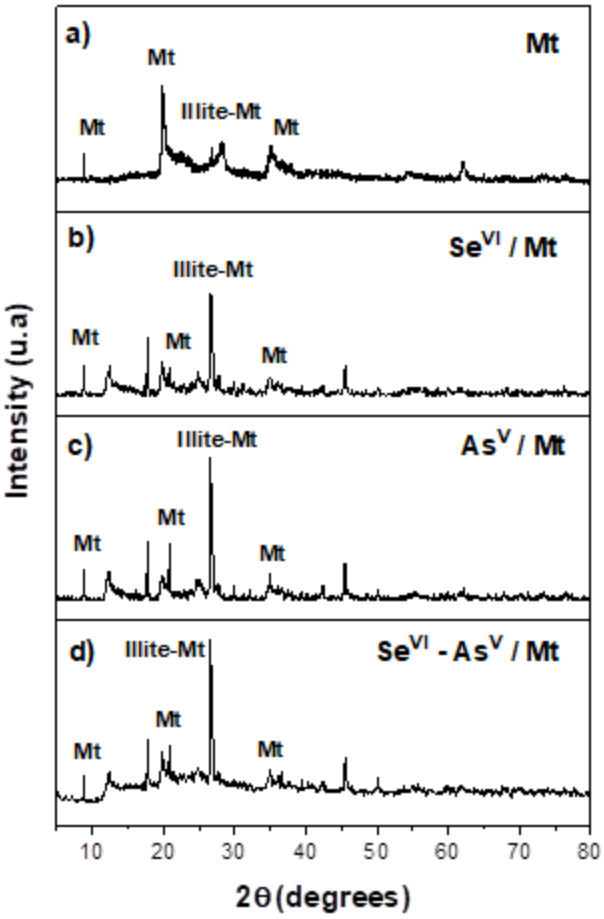

Figure S1. XRD patterns of (a) Mt, (b) Se^{VI} / Mt, (c) As^{V} / Mt, and (d) Se^{VI} - As^{V} / Mt (Mt= Montmorillonite).

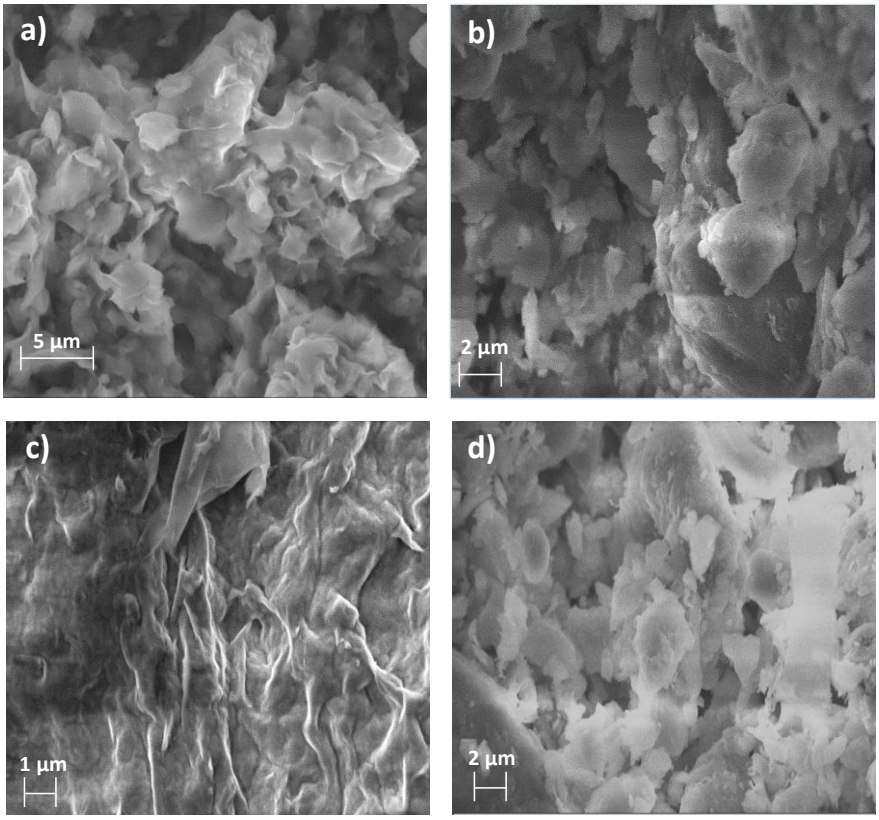

Figure S2. SEM images of (a) Mt, (b) Se^{VI} / Mt, (c) As^{V} / Mt, and (d) Se^{VI} - As^{V} / Mt.

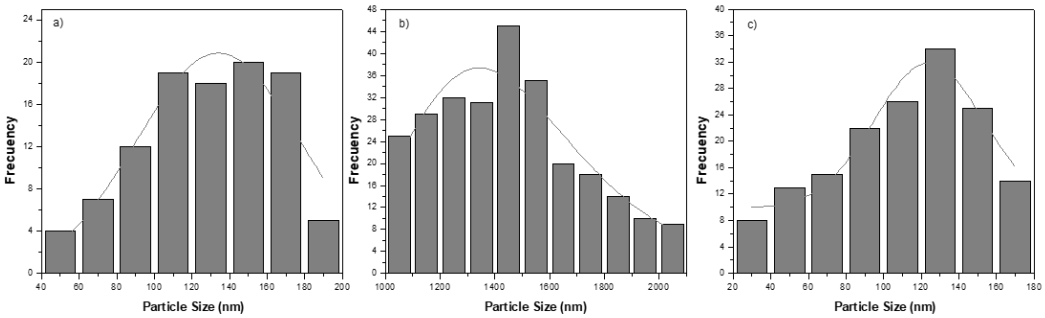

Figure S3. Histograms with the corresponding particle size distribution for (a) NZVI, (b) Mt, and (c) NZVI-Mt.

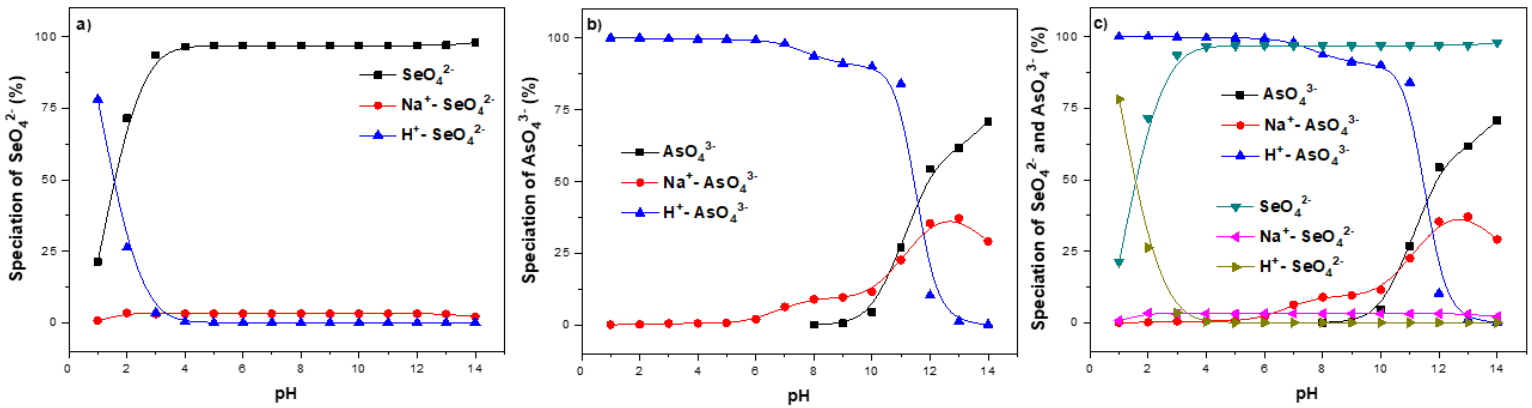

Figure S4. Speciation diagram of (a) Se^{VI} and (b) As^{V} in a monocomponent system, and (c) Se^{VI} - As^{V} in a competitive system, in solution considering the experimental conditions.

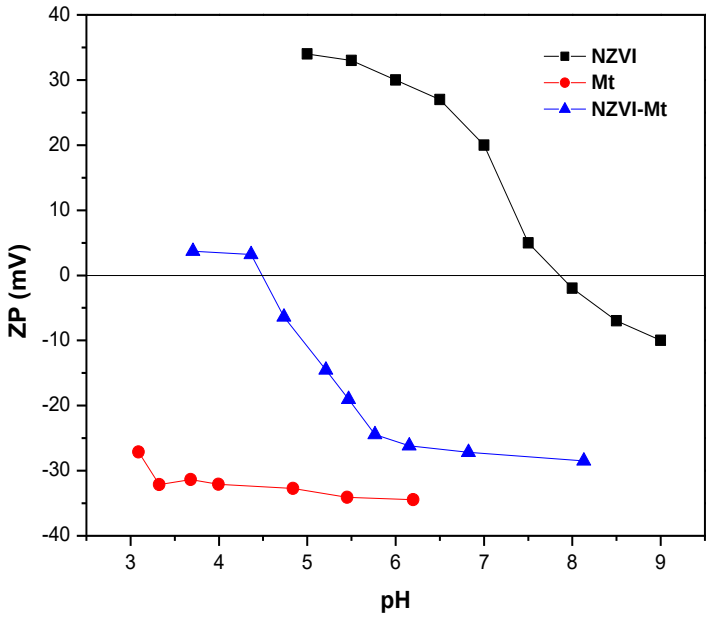

Figure S5. Zeta potential of Mt, NZVI and NZVI-Mt.

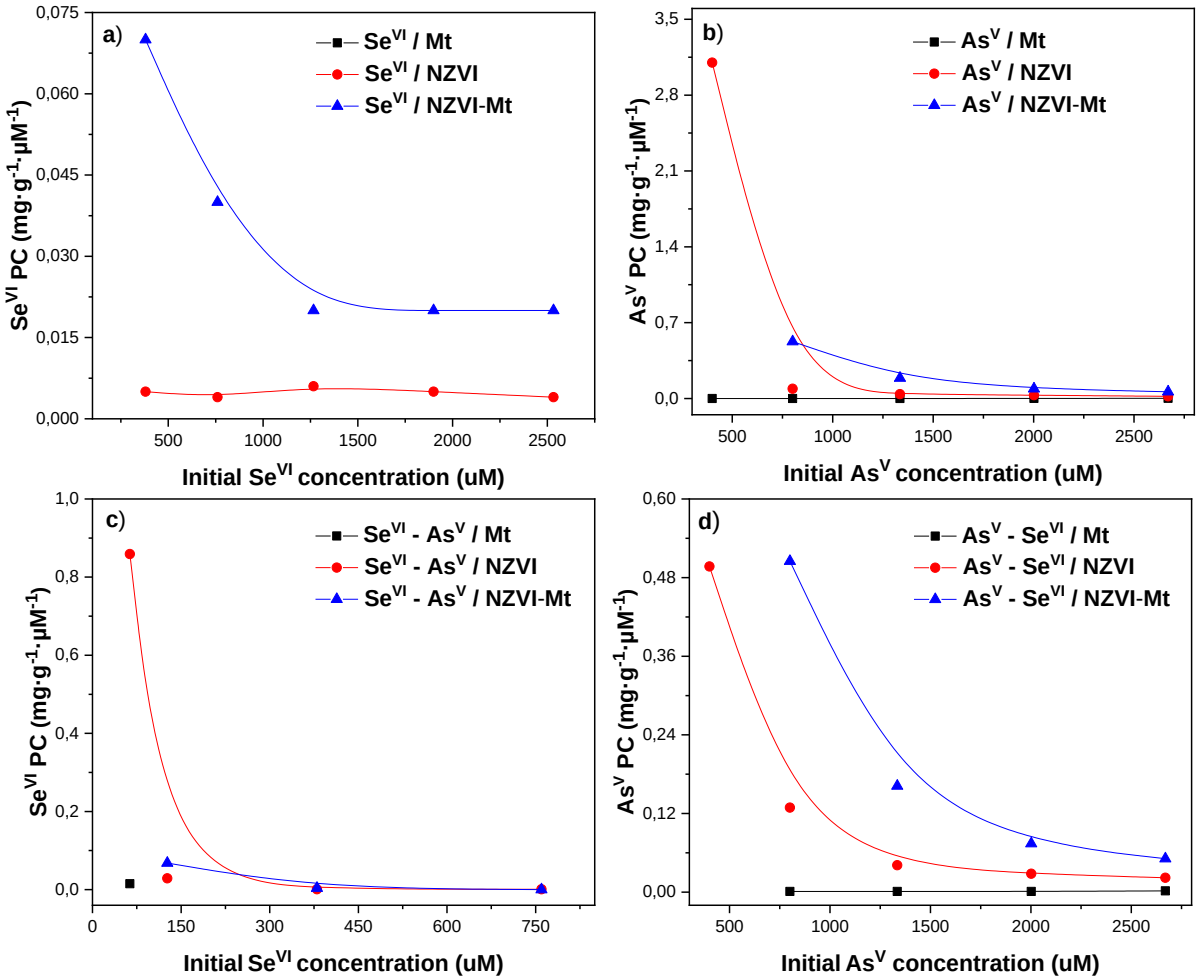

Figure S6. Partition coefficient (PC) for the adsorption of (a) only Se^{VI}, (b) only As^{V}, (c), Se^{VI} - As^{V}, and (d) As^{V} - Se^{VI} on NZVI, MT and NZVI-Mt at different initial concentrations.

Table S1 Kinetic equations used for the description of As^{V}, Se^{VI}, As^{V} - Se^{VI} and Se^{VI} - As^{V} removal.

Kinetic equations	Equation	Linear expression	Parameters	References
Pseudo-first-order (PFO)	$\frac{dq_t}{dt} = k_1(q_e - q_t)$	$\log(q_e - q_t) = \log(q_e) - \frac{k_1}{2.303} x\, t$	q_t = amount of anion adsorbed at any time. q_e = amount of anion adsorbed at equilibrium ($mg \cdot g^{-1}$). k_1 = PFO rate constant (min^{-1}) k_2 = PSO rate constant ($g \cdot mg^{-1} \cdot min^{-1}$)	(Arancibia-miranda et al., 2014; Cáceres-Jensen et al., 2013; Hamdi et al., 2014; Ho and McKay, 1999)
*** Pseudo-second-order (PSO)**	$\frac{dq_t}{dt} = k_2(q_e - q_t)^2$	$\frac{t}{q_t} = \frac{1}{q_e^2 k_2} + \frac{t}{q_e}$		

*From PSO initial adsorption rate (h), can be calculated **by multiplying** $k_2 q_t^2$ ($mg \cdot g^{-1}\ min^{-1}$).

Table S2 Isotherm equations used for the description of As^{V}, Se^{VI}, As^{V} - Se^{VI} and Se^{VI} - As^{V} removal.

Isotherm equations	Equation	Parameters	References
Langmuir	$q_e = \frac{q_m K_L C_e}{1 + K_L C_e}$	q_e = Amount of adsorbed anion per unit mass of the adsorbent at equilibrium ($mg \cdot g^{-1}$) q_{max} = Maximum adsorption capacity ($mg \cdot g^{-1}$). C_e = concentration of anion at equilibrium in the solution ($mg \cdot L^{-1}$). K_L= Constant related to the affinity ($L \cdot mg^{-1}$) K_F = Freundlich adsorption coefficient ($(mg \cdot g^{-1})(L \cdot mg^{-1})^{1/n}$); Adsorption intensity ($1 < n < 10$)	(Baldikova et al., 2020; Camacho et al., 2011; Kanel et al., 2005)
Freundlich	$q_e = K_F C_e^{1/n}$		

Table S3 Specific surface area for Mt, NZVI and NZVI-Mt.

BET-specific surface area	**Mt**	**NZVI**	**NZVI-Mt**
$mg^{2} \cdot g^{-1}$	8.2	26.3	209.0

Table S4 Adsorption kinetics of As^{V} and Se^{VI} on NZVI, Mt and NZVI-Mt in mono-component and competitive systems using at initial concentration of 200 mg·L^{-1}.

	As^{V}-Monocomponent system						**As^{V}-Competitive system**					
Time	**NZVI**		**Mt**		**NZVI-Mt**		**NZVI**		**Mt**		**NZVI-Mt**	
(min)	**Ce**	**q_e**	**Ce**	**q_e**	**Ce**	**q_e**	**Ce**	**q_e**	**Ce**	**q_e**	**Ce**	**q_e**
5	160.07	15.94	183.80	6.49	120.67	31.65	161.12	15.51	185.29	5.90	123.46	30.62
10	153.95	18.44	183.86	6.44	101.90	39.29	153.50	18.62	185.44	5.92	107.22	37.11
20	147.60	20.90	183.43	6.79	82.01	47.08	143.01	22.73	183.77	6.16	90.44	43.83
30	143.32	22.65	183.51	7.22	69.50	52.09	142.09	23.12	183.47	6.90	82.19	47.12
45	141.82	23.09	180.58	7.48	63.91	54.00	142.79	22.70	181.88	7.35	70.81	51.68
60	139.40	24.23	181.71	7.40	61.14	55.50	139.57	24.15	182.15	7.32	70.99	51.60
90	137.96	24.92	182.04	7.43	55.61	58.00	133.32	26.78	181.89	7.23	65.35	53.86
120	135.25	25.82	182.24	7.36	51.48	59.25	131.13	27.48	182.62	7.05	65.50	53.80
150	133.55	26.64	181.62	7.37	47.28	61.21	131.54	27.44	181.73	7.32	67.63	52.95
180	134.14	26.36	181.68	7.28	47.39	61.08	132.62	26.97	181.65	7.13	66.73	53.31

	Se^{VI}-Monocomponent system						Se^{VI}-Competitive system					
	Ce	**q_e**	**Ce**	**q_e**	**Ce**	**q_e**	**Ce**	**q_e**	**Ce**	**q_e**	**Ce**	**q_e**
5	190.57	3.77	200	0.00	182.38	7.05	197.83	0.87	200	0.00	200	0.00
10	190.99	3.60	200	0.00	175.28	9.89	197.36	1.06	200	0.00	200	0.00
20	190.66	3.74	200	0.00	175.07	9.97	197.21	1.12	200	0.00	200	0.00
30	190.93	3.63	200	0.00	172.81	10.88	196.42	1.43	200	0.00	200	0.00
45	190.94	3.62	200	0.00	174.11	10.36	197.05	1.18	200	0.00	200	0.00
60	190.24	3.91	200	0.00	173.29	10.68	196.58	1.37	200	0.00	200	0.00
90	190.18	3.93	200	0.00	172.88	10.85	196.99	1.21	200	0.00	200	0.00
120	190.11	3.95	200	0.00	172.69	10.93	196.84	1.27	200	0.00	200	0.00
150	190.22	3.91	200	0.00	172.74	10.90	196.92	1.23	200	0.00	200	0.00
180	190.16	3.94	200	0.00	172.79	10.88	196.67	1.33	200	0.00	200	0.00

Ce = equilibrium solution concentration ($mg \cdot L^{-1}$); qe = experimental adsorption capacity ($mg \cdot g^{-1}$).

Table S5 As^{V} and Se^{VI} adsorption capacities and partition coefficients (PC) of the tested adsorbents at initial concentration of 200 mg·L^{-1} at different times of reaction.

	As^{V}-Monocomponent system									**As^{V}-Competitive system**								
	Mt			NZVI			NZVI-Mt			Mt			NZVI			NZVI-Mt		
TR	%	q_e	PC	%	q_e	PC	%	q_e	PC	%	q_e	PC	%	q_e	PC	%	q_e	PC
5	8.1	6.49	0.0026	20.0	15.94	0.007	39.7	31.65	0.020	7.4	5.90	0.0024	19.4	15.51	0.007	38.3	30.62	0.019
30	8.0	6.44	0.0026	23.0	18.44	0.009	49.1	39.29	0.029	7.4	5.92	0.0024	23.3	18.62	0.009	46.4	37.11	0.026
20	8.5	6.79	0.0028	26.2	20.90	0.011	59.0	47.08	0.043	7.8	6.16	0.0025	28.5	22.73	0.012	54.8	43.83	0.036
30	9.1	7.22	0.0030	28.3	22.63	0.012	65.3	52.09	0.056	8.6	6.90	0.0028	29.0	23.12	0.012	58.9	47.12	0.043
45	9.4	7.48	0.0031	29.1	23.09	0.012	68.1	54.00	0.063	9.3	7.35	0.0030	28.6	22.70	0.012	64.6	51.68	0.055
60	9.2	7.40	0.0031	30.3	24.23	0.013	69.4	55.50	0.068	9.1	7.32	0.0030	30.2	24.50	0.013	64.5	51.60	0.054
90	9.3	7.43	0.0031	31.0	24.92	0.014	72.2	58.00	0.078	9.1	7.23	0.0030	33.3	26.78	0.015	67.3	53.86	0.062
120	9.3	7.36	0.0030	32.4	25.82	0.014	74.3	59.25	0.086	8.9	7.05	0.0029	34.4	27.48	0.016	67.3	53.80	0.062
150	9.2	7.37	0.0030	33.2	26.64	0.015	76.4	61.21	0.097	9.1	7.32	0.0030	34.2	27.44	0.016	66.2	52.95	0.059
180	9.1	7.28	0.0030	32.9	26.36	0.015	76.3	61.08	0.097	9.0	7.13	0.0029	33.7	26.97	0.015	66.6	53.31	0.060

	Se^{VI}-Monocomponent system									Se^{VI}-Competitive system								
	Mt			NZVI			NZVI-Mt			Mt			NZVI			NZVI-Mt		
TR	%	q_e	PC	%	q_e	PC	%	q_e	PC	%	q_e	PC	%	q_e	PC	%	q_e	PC
5	ND	ND	ND	4.7	3.77	0.0016	8.81	7.05	0.003	ND	ND	ND	1.1	0.87	0.0003	ND	ND	ND
30	ND	ND	ND	4.5	3.60	0.0015	12.36	9.89	0.004	ND	ND	ND	1.3	1.06	0.0004	ND	ND	ND
20	ND	ND	ND	4.7	3.74	0.0015	12.47	9.97	0.004	ND	ND	ND	1.4	1.12	0.0004	ND	ND	ND
30	ND	ND	ND	4.5	3.63	0.0015	13.60	10.88	0.005	ND	ND	ND	1.8	1.43	0.0006	ND	ND	ND
45	ND	ND	ND	4.5	3.62	0.0015	12.95	10.36	0.005	ND	ND	ND	1.5	1.18	0.0005	ND	ND	ND
60	ND	ND	ND	4.9	3.91	0.0016	13.35	10.68	0.005	ND	ND	ND	1.7	1.37	0.0005	ND	ND	ND
90	ND	ND	ND	4.9	3.93	0.0016	13.56	10.85	0.005	ND	ND	ND	1.5	1.21	0.0005	ND	ND	ND
120	ND	ND	ND	4.9	3.95	0.0016	13.66	10.93	0.005	ND	ND	ND	1.6	1.27	0.0005	ND	ND	ND
150	ND	ND	ND	4.9	3.91	0.0016	13.63	10.90	0.005	ND	ND	ND	1.5	1.23	0.0005	ND	ND	ND
180	ND	ND	ND	4.9	3.94	0.0016	13.61	10.88	0.005	ND	ND	ND	1.7	1.33	0.0005	ND	ND	ND

TR = time of reaction; % = removal efficiency; q_e = experimental adsorption capacity ($mg \cdot g^{-1}$); PC = partition coefficient ($mg \cdot g^{-1} \cdot \mu M^{-1}$); ND = not determined.

Table S6 Equilibrium solution concentration measured and adsorption capacity obtained for the adsorption isotherms of As^{V} and Se^{VI} on Mt, NZVI and NZVI-Mt in mono-component and competitive systems.

	As^{V} Mono-component system						**Se^{VI} Mono-component system**					
C_0	Mt		NZVI		Mt-nZVI		Mt		NZVI		Mt-nZVI	
	Ce	**q_e**	**Ce**	**q_e**	**Ce**	**q_e**	**Ce**	**q_e**	**Ce**	**q_e**	**Ce**	**q_e**
0.5	0.00	0.20	0.00	0.20	0.00	0.20	0.00	0.20	0.25	0.10	0.00	0.20
1	0.00	0.40	0.00	0.40	0.00	0.40	0.00	0.40	0.00	0.40	0.00	0.40
5	3.59	0.56	0.00	1.99	0.00	1.99	4.37	0.25	2.30	1.08	0.00	2.00
10	9.30	0.28	0.00	3.99	0.00	3.99	9.91	0.04	6.01	1.60	0.00	4.01
30	30.00	0.00	0.28	11.79	0.00	11.91	30.00	0.00	25.58	1.78	9.73	8.10
60	60.00	0.00	14.46	18.20	3.24	22.69	60.00	0.00	52.92	2.82	28.08	12.73
100	100.00	0.00	42.77	22.99	13.72	34.65	100.00	0.00	84.25	6.29	64.29	14.27
150	145.71	1.71	80.21	27.85	37.38	44.93	150.00	0.00	129.21	8.31	96.49	21.56
200	187.28	5.10	123.66	30.60	65.50	53.91	200.00	0.00	176.23	9.46	134.13	26.49

	As^{V} Competitive system						Se^{VI} Competitive system					
	Ce	**q_e**	**Ce**	**q_e**	**Ce**	**q_e**	**Ce**	**q_e**	**Ce**	**q_e**	**Ce**	**q_e**
0.5	0.00	0.20	0.00	0.20	0.00	0.20	0.00	0.20	0.00	0.20	0.00	0.20
1	0.00	0.40	0.00	0.40	0.00	0.40	0.00	0.40	0.00	0.40	0.00	0.40
5	3.77	0.49	0.00	2.00	0.00	2.00	3.35	0.66	0.18	1.92	0.00	2.00
10	10	0.00	0.00	4.01	0.00	3.98	10	0.00	5.23	1.91	3.18	2.73
30	30	0.00	1.71	11.32	0.00	11.98	30	0.00	29.43	0.23	26.73	1.31
60	57.92	0.83	11.33	19.45	3.36	22.64	60	0.00	58.40	0.63	59.41	0.23
100	97.72	0.91	42.42	22.99	15.61	33.69	100	0.00	100.00	0.00	100	0.00
150	145.41	1.83	77.08	29.07	43.13	42.61	150	0.00	150.00	0.00	150	0.00
200	186.63	5.36	116.07	33.62	73.82	50.54	200	0.00	200.00	0.00	200	0.00

C_0 = initial solution concentration ($mg \cdot L^{-1}$); Ce = equilibrium solution concentration ($mg \cdot L^{-1}$); q_e = experimental adsorption capacity ($mg \cdot g^{-1}$).

Table S7 As^{V} and Se^{VI} adsorption capacities and partition coefficients (PC) for the adsorbents at different concentration levels.

	As^{V}-Mono-component system									**As^{V}-Competitive system**								
	NZVI			**Mt**			**NZVI-Mt**			**NZVI**			**Mt**			**NZVI-Mt**		
C_0	**%**	**q_e**	**PC**	**%**	**q_e**	**PC**	**%**	**q_e**	**PC**	**%**	**q_e**	**PC**	**%**	**q_e**	**PC**	**%**	**q_e**	**PC**
0.5	100	0.20	-----	100	0.20	-----	100	0.20	-----	100	0.20	-----	100.0	0.20	-----	100	0.20	-----
1	100	0.40	-----	100	0.40	-----	100	0.40	-----	100	0.40	-----	100.0	0.40	-----	100	0.40	-----
5	100	1.99	-----	28.3	0.56	0.012	100	1.99	-----	100	2.00	-----	24.7	0.49	-----	100	2.00	-----
10	100	3.99	-----	7.0	0.28	0.002	100	3.99	-----	100	4.01	-----	0.0	0.00	-----	100	3.98	-----
30	99.1	11.79	3.12	0.0	0.00	0.000	100	11.91	-----	94.3	11.32	0.497	0.0	0.00	-----	100	98	-----
60	75.9	18.20	0.09	0.0	0.00	0.000	94.6	22.69	0.525	81.1	19.45	0.129	3.5	0.83	0.001	94.4	22.64	0.505
100	57.2	22.99	0.04	0.0	0.00	0.000	86.3	34.65	0.189	57.6	22.99	0.041	2.3	0.91	0.001	84.4	33.69	0.162
150	46.5	27.85	0.03	2.9	1.71	0.001	75.1	44.93	0.090	48.6	29.07	0.028	3.1	1.83	0.001	71.2	42.61	0.074
200	38.2	30.60	0.02	6.4	5.10	0.002	67.3	53.91	0.062	42.0	33.62	0.022	6.7	5.36	0.002	63.1	50.54	0.051

	Se^{VI}-Mono-component system									Se^{VI}-Competitive system								
	NZVI			**Mt**			**NZVI-Mt**			**NZVI**			**Mt**			**NZVI-Mt**		
C_0	**%**	**q_e**	**PC**	**%**	**q_e**	**PC**	**%**	**q_e**	**PC**	**%**	**q_e**	**PC**	**%**	**q_e**	**PC**	**%**	**q_e**	**PC**
0.5	50.0	0.10	0.032	100	0.20	-----	100	0.20	-----	100	0.20	-----	100	0.20	-----	100	0.20	------
1	100	0.40	-----	99.7	0.40	9.438	100	0.40	-----	100	0.40	-----	100	0.40	-----	100	0.40	-----
5	54.0	1.08	0.037	12.7	0.25	0.005	100	2.00	-----	96.5	1.92	0.859	33.0	0.66	0.02	100	2.00	-----
10	39.9	1.60	0.021	0.9	0.04	0.000	100	4.01	-----	47.7	1.91	0.029	0.0	0.00	-----	68.2	2.73	0.068
30	14.7	1.78	0.005	0.0	0.00	-----	67.6	8.10	0.07	1.9	0.23	0.001	0.0	0.00	-----	10.9	1.31	0.004
60	11.8	2.82	0.004	0.0	0.00	-----	53.2	12.73	0.04	2.7	0.63	0.001	0.0	0.00	-----	1.0	0.23	0.000
100	15.8	6.29	0.006	0.0	0.00	-----	35.7	14.27	0.02	0.0	0.00	-----	0.0	0.00	-----	0.0	0.00	-----
150	13.9	8.31	0.005	0.0	0.00	-----	35.7	21.56	0.02	0.0	0.00	-----	0.0	0.00	-----	0.0	0.00	-----
200	11.9	9.46	0.004	0.0	0.00	-----	32.9	26.49	0.02	0.0	0.00	-----	0.0	0.00	-----	0.0	0.00	-----

C_0 = initial solution concentration ($mg \cdot L^{-1}$); % = removal efficiency; q_e = experimental adsorption capacity ($mg \cdot g^{-1}$); PC = partition coefficient ($mg \cdot g^{-1} \cdot \mu M^{-1}$).

References

Arancibia-Miranda, N., Baltazar, S.E., García, A., Muñoz-Lira, D., Sepúlveda, P., Rubio, M.A., Altbir, D., 2016. Nanoscale zero valent supported by zeolite and montmorillonite: Template effect of the removal of lead ion from an aqueous solution. J. Hazard. Mater. 301, 371–380.

Arancibia-miranda, N., Baltazar, S.E., García, A., Romero, A.H., Rubio, M.A., Altbir, D., 2014. Lead removal by nano-scale zero valent iron : Surface analysis and pH effect. Mater. Res. Bull. 59, 341–348.

Baldikova, E., Pospiskova, K., Safarik, I., 2020. Removal of bisphenol A using magnetically responsive spruce chip biochar. Chem. Eng. Technol. 43, 168–171.

Boparai, H.K., Joseph, M., Carroll, D.M.O., 2011. Kinetics and thermodynamics of cadmium ion removal by adsorption onto nano zerovalent iron particles. J. Hazard. Mater. 186, 458–465.

Cáceres-Jensen, L., Rodríguez-Becerra, J., Parra-Rivero, J., Escudey, M., Barrientos, L., Castro-Castillo, V., 2013. Sorption kinetics of diuron on volcanic ash derived soils. J. Hazard. Mater. 261, 602–613.

Camacho, L.M., Parra, R.R., Deng, S., 2011. Arsenic removal from groundwater by MnO2-modified natural clinoptilolite zeolite: Effects of pH and initial feed concentration. J. Hazard. Mater. 189, 286–293Hamdi, W., Pelster, D., Seffen, M., 2014. Phosphorus sorption kinetics in different types of alkaline soils. Arch. Agron. Soil Sci. 60, 577–586.

Hamdi, W., Pelster, D., Seffen, M., 2014. Phosphorus sorption kinetics in different types of alkaline soils. Arch. Agron. Soil Sci. 60, 577–586

Ho, Y.S., McKay, G., 1999. Pseudo-second order model for sorption processes. Process

Biochem. 34, 451–465.

Kanel, S.R., Manning, B., Charlet, L., Choi, H., 2005. Removal of arsenic(III) from groundwater by nanoscale zero-valent iron. Environ. Sci. Technol. 39, 1291–1298.